CrossMark

Three-Dimensional Modeling of Suspension Plasma Spraying with Arc Voltage Fluctuations

E. Dalir[1] · C. Moreau[1] · A. Dolatabadi[1]

Abstract In this study, a three-dimensional DC plasma torch is modeled using Joule effect method to simulate the plasma jet and its voltage fluctuations. The plasma gas is a mixture of argon/hydrogen, and the arc voltage fluctuation is used as an input data in the model. Reynolds stress model is used for time-dependent simulation of the oscillating flow of the plasma gas interacting with the ambient air. The results are used to investigate the plasma oscillation effects on the trajectory, temperature, and velocity of suspension droplets. Suspensions are formed of ethanol and yttria-stabilized zirconia submicron particles and modeled as multicomponent droplets. To track the droplets/particles, a two-way coupled Eulerian–Lagrangian method is employed. In addition, in order to simulate the droplet breakup, Kelvin–Helmholtz/Rayleigh–Taylor (KH–RT) breakup model is used. After the completion of suspension breakup and evaporation, the sprayed particles are tracked to obtain the in-flight particle conditions including trajectory, size, velocity, and temperature. The arc voltage fluctuations were found to cause more than two times wider particle trajectories resulting in wider particle temperature, velocity, and size distributions compared with the case of constant voltage.

Keywords arc voltage fluctuation · suspension plasma spraying · unsteady 3D simulation · yttria-stabilized zirconia (YSZ)

✉ A. Dolatabadi
ali.dolatabadi@concordia.ca

[1] Department of Mechanical, Industrial and Aerospace Engineering, Concordia University, Montreal, QC, Canada

Introduction

For many years, the thermal spray coating technology has been increasingly used to produce more resistant surfaces against corrosion, erosion, and heat and to extend the lifetime of surface properties by rebuilding worn parts instead of replacing the whole component in order to enhance the functional performance of the structural parts in different applications (Ref 1).

In order to have a proper surface coating of submicron-sized particles, a relatively new deposition process, suspension plasma spraying (SPS), has been increasingly used. In the SPS technique, submicron-sized particles are sprayed efficiently to form finely structured coatings (Ref 2-6). To have enough momentum for the fine particles to penetrate into the plasma jet, they are mixed with a liquid carrier (e.g., ethanol or water) to form a suspension that is injected into the plasma.

Ideal results can be obtained when all particles injected into the plasma flow reach the substrate with temperature well above their melting point and below their vaporization point with high enough velocity to be deposited upon impact on the substrate (Ref 7). Therefore, a critical aspect in the SPS process is to well control the suspension droplets trajectories, temperatures, velocities, and their interactions with the plasma flow.

Arc voltage fluctuations, particle mass flow rate, injector angle, and particle size distribution are some of the effective parameters in plasma spraying process. Arc voltage fluctuations cause significant variations of the heat and momentum transfer between the plasma jet and the injected particles (Ref 8, 9). Moreover, using different types of plasma gases such as Ar-H$_2$ and the anode erosion have significant effects on the arc oscillations.

 Springer

There are several numerical simulations performed to predict plasma jet and its interaction with suspension droplets based on the assumption of steady plasma flow. Usually, to simplify the computations, temperature and velocity profiles at the gun exit are used as the inlet boundary condition (Ref 10-17). In order to include the internal plasma flow, a constant volumetric heat source is added to the energy equation to model the heat generated by the arc inside the gun (Ref 18, 19). In this approach, the plasma jet is still in the steady state.

Jabbari et al. (Ref 10) modeled the suspension plasma spraying using nickel powder and ethanol as the solvent. Suspension droplets were injected radially into a 3 MB Sulzer Metco plasma gun and simulated as the multicomponent droplets. The arc fluctuations were neglected and the plasma gas was argon. RSM model was utilized to simulate the plasma gas and its interaction with the sprayed particles. However, the authors also applied k–ε model in the free plasma jet to compare the results with the results of RSM turbulence model. It was shown that the k–ε model gives underestimated values for the high-temperature plasma core. To model the particle breakup, Kelvin–Helmholtz/Rayleigh–Taylor (KH–RT) breakup model which gives reasonable results in the case of high Weber number was used. It was concluded that by increasing the suspension injection velocity, the penetration depth increases and when the injection velocity is too high, the quantity of particles with high temperature decreases.

Jadidi et al. (Ref 11) analyzed the effect of using a flat substrate with the same conditions and assumptions used in (Ref 10) in the SPS process. The effect of the standoff distance on particles properties upon impact in the vicinity of the substrate was investigated. It was shown that many fine particles were diverted due to the stagnation region formed near the substrate. It was also concluded that particles moving near the plasma gas centerline obtain higher velocity and higher temperature and are less affected by the stagnation region.

Recently, the effect of substrate curvature on suspension droplet and particle characteristics, especially near the substrate, was investigated by Pourang et al. (Ref 18). The authors applied the assumptions used in (Ref 10). However, in order to improve the simulation of the high-velocity and the high-temperature plasma gas, a constant volumetric energy source $\left(\frac{\eta_t \mathrm{EI}}{V}\right)$ was introduced inside the torch and added to the energy equation. The suspension contained YSZ particles (10 wt.%) in ethanol and was modeled as multicomponent droplets. The results showed that the finer particles obtain higher temperature and velocity compared with other particles. It was also found that compared with the use of flat substrate, the deposition rate decreases more than 50% on a cylindrical substrate.

Due to the nature of plasma jet and the movement of plasma arc attachment on the anode surface, the arc experiences large fluctuations which results in large arc voltage fluctuations. Since the plasma jet formation is naturally an unsteady phenomenon, the results obtained from the steady simulations may not be able to capture the unsteady characteristics of the flow inside and outside the torch.

In general, there are three methods used to simulate transient plasma jets. The first approach is based on coupling the fluid flow and electromagnetic equations to model the plasma arc flow (Ref 20-24). Following such an approach, Moreau et al. (Ref 23) used a three-dimensional transient model with a nozzle diameter of 7 mm to simulate the oscillating plasma jet. The plasma working gases were Ar-H$_2$ and the voltage fluctuation was in the restrike mode due to the torch operating condition. To simulate the anode root attachment inside the torch, the electromagnetic equations in addition to the mass, momentum, and energy equations were applied. The effect of changing the arc current was investigated in this study, and the results showed a higher maximum velocity at the nozzle exit due to an increase in the arc current. A higher voltage fluctuation frequency was also predicted with the arc current increasing. Although this rigorous approach provides detailed information inside the torch, it is computationally very expensive and time-consuming to couple it with suspension flow including suspension breakup, evaporation, as well as particle heating and melting.

The second approach is based on modeling the plasma jet using the Joule effect method in which a volumetric heat source is added to the energy equation neglecting the effect of electromagnetic fields. Although by using this method, the simulation of the arc attachment inside the torch is impossible, a good estimation of the plasma jet fluctuations can be obtained and used for the SPS process modeling. For example, Meillot et al. (Ref 25) simulated a three-dimensional DC plasma jet based on the Joule effect method by introducing a time-dependent volumetric heat source inside the plasma torch. The validation criterion was the thermal efficiency through adjusting the length of the plasma column inside the torch. They showed that the calculated properties of the plasma jet on the centerline, especially near the gun exit, were in good agreement with the experimental values.

In the third approach, the unsteady velocity and temperature profiles can be used as the inlet boundary to simulate the unsteady plasma jet (Ref 26, 27). Meillot et al. (Ref 26) employed the unsteady temperature and velocity profiles at the torch exit as the inlet boundary to simulate the unsteady plasma flow using large eddy simulation (LES) turbulence model. Their focus was modeling the plasma flow interaction with a moving substrate to

investigate the heat transfer to the substrate and consider different standoff distances to evaluate the flow structure in the impingement zone of ceramic particles. The results showed that the presence of the substrate at different standoff distances has significant implications on the plasma flow parameters compared with a free jet.

The aim of the current study is to numerically model the unsteady SPS process taking into account the fluctuations of the plasma jet. For this purpose, an approach similar to the one introduced by Meillot et al. (Ref 25) using a fluctuating volumetric heat source is employed to model the unsteady plasma jet. Swirling flow as well as suspension interaction with the oscillating plasma jet is modeled for more realistic prediction of particle in-flight conditions in SPS process. The developed model is used to investigate the influence of key phenomena and spray parameters.

Geometry and Operating Conditions

A 3 MB Oerlikon Metco gun with a 32.2-mm-long and 5.5-mm-diameter nozzle is used in this study (Fig. 1). The nozzle length in the straight part is 22.5 mm. The cathode and the gas inlet having an angle of 45° which causes swirling flow in the plasma jet are considered in the simulation. Geometry and computational domain of the study employed in the simulations are shown in Fig. 1. The gas inlet diameter is 3.6 mm. The outlet domain is an incomplete cone with initial and final diameters of 60 and 100 mm, respectively, and a length of 140 mm (see Fig. 2). The length of the outlet domain is selected in order to have an extended domain to perform various turbulence models including LES, as well as to comprise distances of more than 60 mm for future comparison with experimental
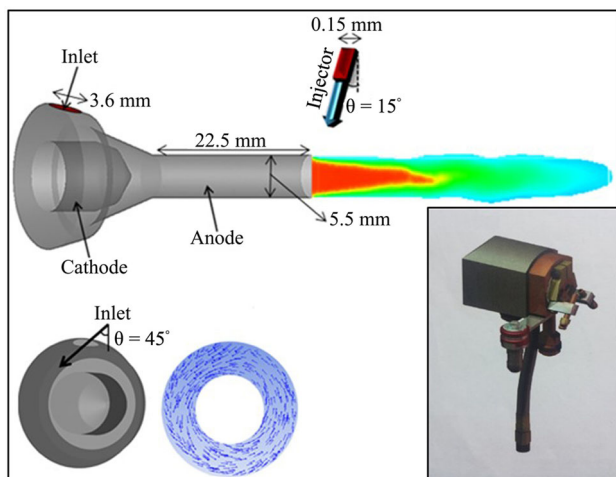
measurements. Indeed, in-flight particle diagnostics can be performed more easily at longer standoff distances.

The plasma working gas is Ar-H$_2$ with a total mass flow rate of 50 slpm and the mean power of 30.6 kW. Torch operating conditions including the thermal efficiency value (58%) acquired from experiments are given in Table 1. These parameters were selected based on previous experimental work for deposition of YSZ coatings carried out in our laboratory. The typical arc voltage fluctuations recorded on the plasma torch during spraying and thermodynamic and transport properties of plasma gases (Ref 28) are used to model the plasma jet. Suspension droplets are formed of YSZ submicron particles and ethanol as the solvent with the feed rate of 22 g/min and the velocity of 24.4 m/s. The thermo-physical properties of YSZ and ethanol used in this study are given in Table 2 (Ref 18, 29).

Mathematical Modeling

Throughout this study, the term quasi-steady is used for the swirling plasma jet without voltage fluctuations, and unsteady plasma jet means the case with both swirl and voltage fluctuations. Similarly, the terms droplets and particles are used for the suspension droplets and particles (solid or molten YSZ), respectively.

A mesh sensitivity analysis was performed for the continuous phase in the quasi-steady state. The procedure involved increasing the number of cells until no further
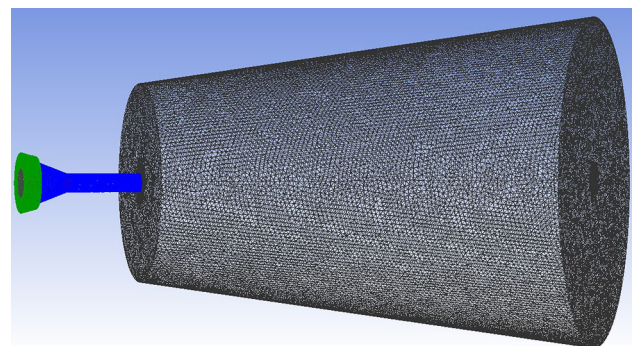
Fig. 2 Computational mesh of the domain of study

Table 1 Operating condition for plasma spraying simulation

Operating condition	Magnitude
Current input, A	600
Average voltage, V	51
Thermal efficiency, %	58
Ar/H$_2$ gas flow rate, slpm	47.5/2.5

Fig. 1 Geometry of the domain of study and direction of inlet flow

changes in the velocity and temperature evolutions along the centerline were observed. The optimum number of cells to reduce the computational cost and time of the modeling contained about 800,000 cells, which were a mixture of tetrahedral and hexahedral volume meshes. The cell sizes were locally refined in the plasma core area inside and outside the gun to capture the large plasma temperature and velocity gradients. Figures 2 and 3 illustrate the mesh sizes used in the study domain.

The plasma is assumed in local thermodynamic equilibrium and optically thin. Mass flow rate and pressure outlet conditions are used for the inlet and outlet boundaries, respectively. The anode wall temperature is fixed at 300 K as the anode nozzle is water cooled during the torch operation. Owing to the RSM turbulence model's capability to consider the effects of streamline curvature, swirl, and rotation, it is used to model the turbulence plasma flow (Ref 30). The governing equations, which are continuity, momentum, energy, and species transport, are solved by ANSYS-Fluent commercial software (Ref 30).

The radiation losses, as shown in Fig. 4, are calculated using the net emission coefficient (Ref 25) and introduced by using a sink term in the energy equation. Figure 5(a)
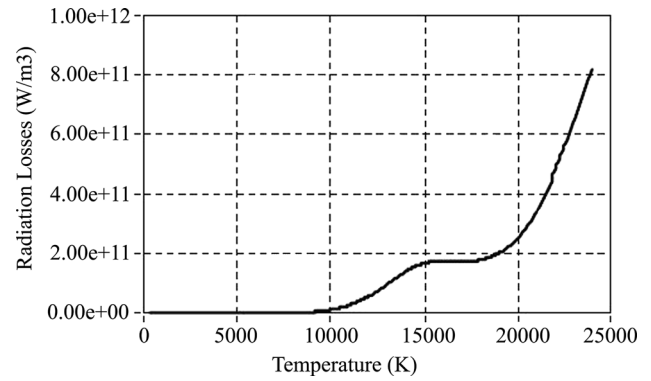

Fig. 4 Radiation losses vs. temperature for argon/hydrogen mixture (Ref 25)
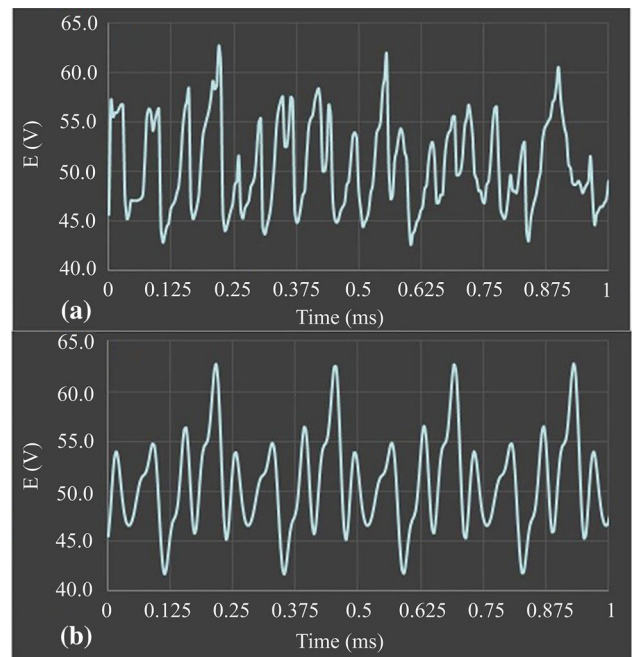
Fig. 5 Arc voltage fluctuations Ar_H₂ (a) typical, (b) modeled with Fourier series

Table 2 Thermo-physical properties of suspension components (Ref 18, 29)

Property	Ethanol	Yttria-stabilized zirconia
Density, kg/m^3	790	5890
Viscosity, kg/m s	0.0012	0.038285
Melting latent heat, J/kg	…	7.06×10^5
Boiling latent heat, J/kg	855237	9×10^6
Melting point, K	…	2988
Boiling point, K	351	5273
Surface tension, N/m	0.022348	1.5

Fig. 3 Finer mesh inside the plasma gun
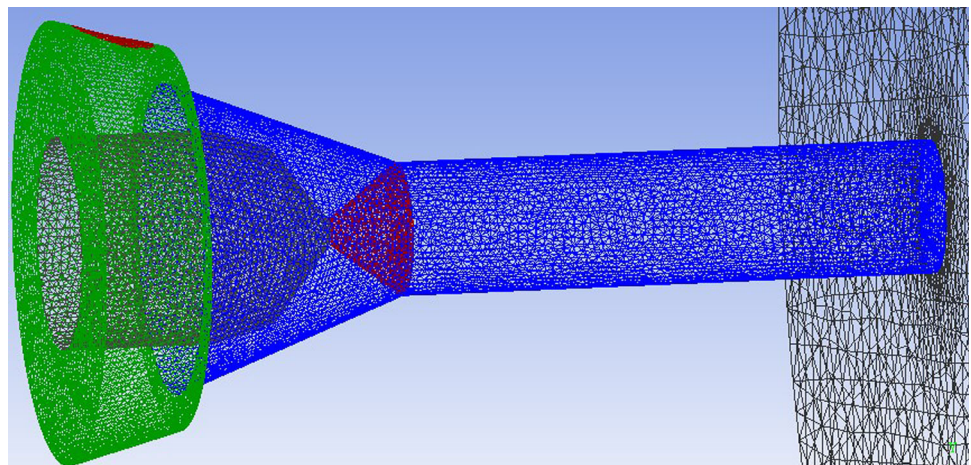
illustrates the typical arc voltage fluctuations recorded on the plasma torch during spraying. In this study, a Fourier series is used to create a periodic function (Fig. 5b) with similar characteristics,

$$E(t) = a_0 + \sum_{n=1}^{8} a_n \cos(n\omega t) + \sum_{m=1}^{8} b_m \sin(m\omega t), \quad \text{(Eq 1)}$$

where $E(t)$ is the arc voltage, a_0 is the average voltage, and $a_1, \ldots, a_n$, $b_1, \ldots, b_n$, and ω are the function coefficients (Table 3). As a result, arc voltage oscillates between 42 and 63 V with a fundamental frequency of 4167 Hz.

In order to model the plasma jet, at first in the steady state, Joule effect is taken into account on the cone volume (V_1) and the cylinder heating zone inside the torch (V_2) to find the mean value of the length (L_m) corresponding to the mean power (Fig. 6). In this case, arc voltage oscillations which result in axial fluctuations are not considered in the simulation. However, there are still azimuthal fluctuations due to the plasma swirling flow.

The obtained results from the quasi-steady case are validated by comparing the thermal efficiency from Eq 2 (Ref 25) and the experimentally measured thermal efficiency,

$$\eta = 1 - \left(\frac{H_{\text{conv}} + H_{\text{rad}}}{P_m} \right), \quad \text{(Eq 2)}$$

where P_m, H_{conv}, and H_{rad} are the average input power, the convection losses, and the radiation losses inside the torch, respectively. H_{conv} is obtained from the numerical results, and H_{rad} is calculated from Fig. 4. After several try-and-error calculations, the average length value is obtained as a length of 16 mm from the cathode tip.

The quasi-steady case results are used to model the unsteady plasma jet. In the unsteady state, the voltage fluctuations presented in Fig. 5 are used as input data to obtain the time-varying length, $L_2(t)$, as schematically shown in Fig. 7,

$$L_2(t) = aE(t) + b, \quad \text{(Eq 3)}$$

where a and b are the constants obtained from $L_{\min}$ and $L_{\max}$ corresponding to $E_{\min}$ and $E_{\max}$. $E(t)$ is the arc voltage fluctuation derived from Fig. 5.

To simulate the heat generated by the fluctuating plasma, volumetric heat sources are introduced inside the plasma torch and added to the energy equation. As shown in Fig. 7, $L_1 (= 3\,\text{mm})$ and volume 1 (V_1) are constant, while volume 2 (V_2) is time dependent as defined in the following equations (Ref 25),

$$\begin{cases} P_1 = \dfrac{P_m}{L_m} L_1 & \rightarrow \quad S_{h1} = \dfrac{P_1}{V_1} = C_1 \\ P_2(t) = \dfrac{P_m}{L_m} L_2(t) & \rightarrow \quad S_{h2} = \dfrac{P_2(t)}{V_2(t)} = C_2 \end{cases}, \quad \text{(Eq 4)}$$

$$P = \text{EI}, \quad \text{(Eq 5)}$$

where L_m is the average length corresponding to the mean power (P_m), P_1 and S_{h1} are the power and the volumetric heat source of V_1, respectively, and P_2 and S_{h2} are the power and the volumetric heat source of V_2, respectively.

After modeling the plasma jet, the converged results are used to investigate the effect of plasma oscillations on the trajectory, temperature, and velocity of the injected suspension droplets which are modeled as multicomponent droplets.

Table 3 Coefficients of modeled voltage fluctuations function

a_0	a_1	a_2	a_3	a_4	a_5	a_6	a_7	a_8
50.84	2.1280	-1.15580	1.29060	-3.9420	-0.6230	-1.13420	-1.79220	-0.106340

w	b_1	b_2	b_3	b_4	b_5	b_6	b_7	b_8
$2.63e^{+04}$	-1.79520	-2.350	-1.51720	1.0490	1.11620	0.58580	-0.194180	1.5320

Fig. 6 Plasma torch with invariant heating zones V_1 and V_2 (quasi-steady case)
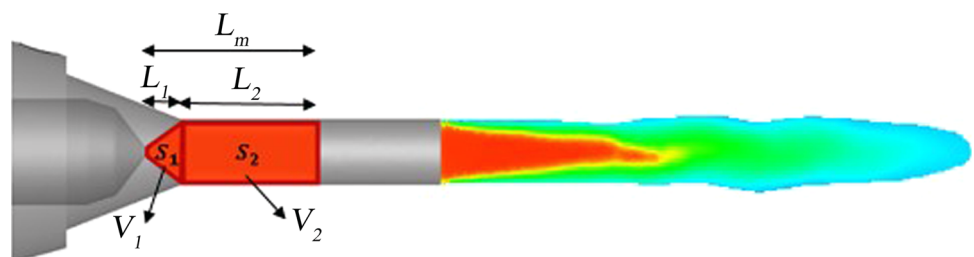
Figure 8 illustrates the multicomponent assumption approach compared with the more realistic suspension evolution (Ref 10). Suspension droplets start to break up and then evaporate as soon as they interact with the continuous phase (plasma jet). A Lagrangian approach including coupling with the continuous phase is used for the discrete-phase modeling. The concentration of suspension is assumed to be constant during the droplet breakup as the timescale associated with the breakup is much smaller than that of the droplet evaporation. The diffusion of ethanol in the plasma is not considered in this study (no chemical reaction).
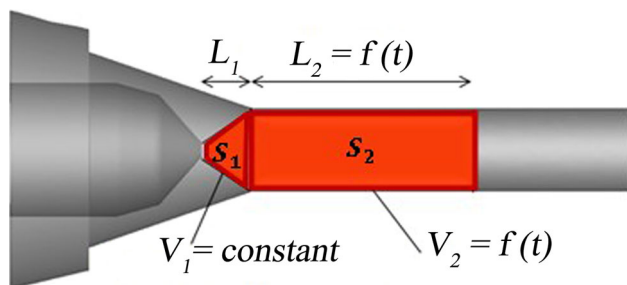
Fig. 7 Plasma torch with the heating zones V_1 and $V_2(t)$ (unsteady case)

To model the droplet fragmentation due to the presence of catastrophic breakup inside the plasma plume (We > 300), the KH–RT breakup model in which the Kelvin–Helmholtz (KH) waves combine with the Rayleigh–Taylor (RT) instabilities on the droplet surface is used (Ref 4). In the KH–RT model, the KH waves are used to predict the primary fragmentation inside a liquid core.

Then, the secondary breakup of the individual droplets shed from the liquid is modeled with both KH and RT instabilities. In both mechanisms, the droplet breakup is modeled by tracking the wave growth on the droplet surface. Generally, for high Weber number sprays, RT instabilities grow faster because of the high droplet acceleration and become dominant outside the liquid core (Ref 30).

In this study, in order to model the primary atomization, similar to the work of Pourang et al. (Ref 18), suspension injection in the form of a continuous jet is substituted with a chain of fragmented droplets with a uniform size of 150 μm (equal to the injector diameter) injected radially with a reverse angle of $\theta = 15°$ with respect to the normal plane to the plasma jet axis as schematically shown in Fig. 9. Droplets are injected every 1 μs corresponding to a suspension mass flow rate of 22 g/min. Then, the child droplets ejected from the continuous jet are modeled using the KH–RT instabilities. There is no limitation for the droplets breakup, and as long as they satisfy the criteria for
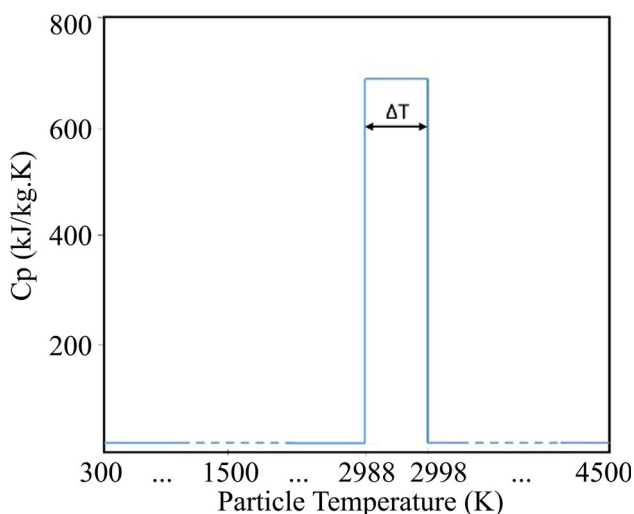

Fig. 8 Realistic mechanism of suspension droplet progress compared to the multicomponent approach (Ref 10)

Fig. 9 Schematic of injected droplets into the plasma jet

Fig. 10 Specific heat of particles with modifications to account for latent heat of fusion (Ref 18)

the breakup, it is continued and a new generation of the child droplets appears in the domain.

To predict the particle dispersion due to the fluid-phase turbulence, a model called the stochastic tracking model (Ref 30) is used. This model, which is a random walk model, is applied by including the instantaneous turbulent velocity fluctuations on the particle trajectories. The energy equation of the multicomponent droplet is calculated as (Ref 30),

$$m_p c_p \frac{dT_p}{dt} = hA_p(T_\infty - T_p) + \sum_i \frac{dm_i}{dt}(h_{\text{vap},i}), \qquad \text{(Eq 6)}$$

where c_p, A_p, and T_p are the droplet specific heat, surface area, and temperature, respectively. T_∞ is the continuous-phase (plasma jet in this study) temperature, $h_{\text{vap},i}$ is the latent heat of component i, and h is the convective heat transfer coefficient. The effect of radiation heat transfer is neglected.

The specific heat of the particles during melting is calculated as (Ref 18),

$$C_p \times \Delta T = H_f, \qquad \text{(Eq 7)}$$

where C_p is the particle specific heat and H_f is the particle fusion enthalpy. Figure 10 shows the applied method in which ΔT is assumed to be 10 K. To find the convective heat and mass transfer coefficients, Nusselt and Sherwood numbers obtained from Ranz and Marshall correlations (Ref 30) are used.

Results and Discussion

The focus of this study is to model the unsteady plasma jet due to the voltage fluctuations and to investigate the effects of those oscillations on in-flight particles properties (temperature, velocity, size, and trajectory). To do so, in the first step, a quasi-steady plasma flow (no voltage fluctuation) is modeled, and then to validate the results, they are compared with other studies. In a second step, the unsteady plasma jet considering the voltage fluctuations is simulated and the results are used for the SPS process modeling. The obtained results are discussed to observe the effect of unsteady plasma flow on the in-flight particle properties. The effect of changing the suspension feed rate on the in-flight particles characteristics is also discussed. Finally, to see the effect of the arc voltage fluctuations on the SPS process, the results obtained from the unsteady plasma jet are compared with the case in the absence of voltage fluctuations (quasi-steady case).

Quasi-Steady Plasma Flow

In the quasi-steady state, considering the thermal efficiency value (58%) acquired from the experimental data and the value of mean power (30.6 kW), L_2 and L_m are obtained as 13 and 16 mm, respectively. The resulting plasma gas temperature and velocity fields are illustrated in Fig. 11(a) and (b), respectively. The asymmetric gas flow field shown in Fig. 11 is the result of the azimuthal fluctuations due to the swirling flow.

In order to validate the plasma jet model, the results obtained from this study are compared with the numerical results in (Ref 18) and also the experimental works of (Ref 31, 32). In (Ref 18), RSM model was used to simulate a steady plasma flow with Ar_H2 as the plasma forming gases. In (Ref 31), the author applied the spectroscopic measurements to obtain the highest temperature and the enthalpy probe to measure the lowest ones. Furthermore, plasma light fluctuation measurements were used to obtain the velocity values. Figures 12 and 13 represent the evolution of the plasma gas temperature and velocity along the centerline. The calculated temperature and velocity values cannot be compared directly to those reported in (Ref 18, 31, 32) due to the different operating conditions and nozzle geometry used in this study. However, the results showed good agreement in the trend of the temperature and velocity evolution.

Fig. 11 Quasi-steady state plasma gas (a) temperature and (b) velocity contours
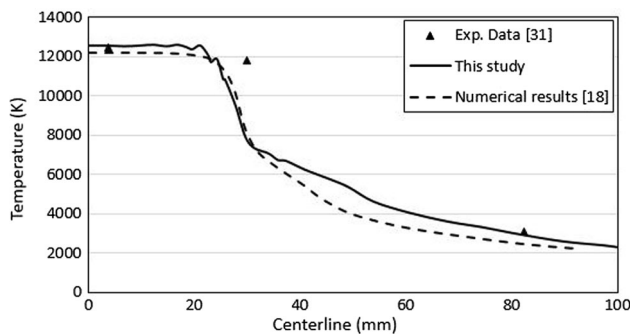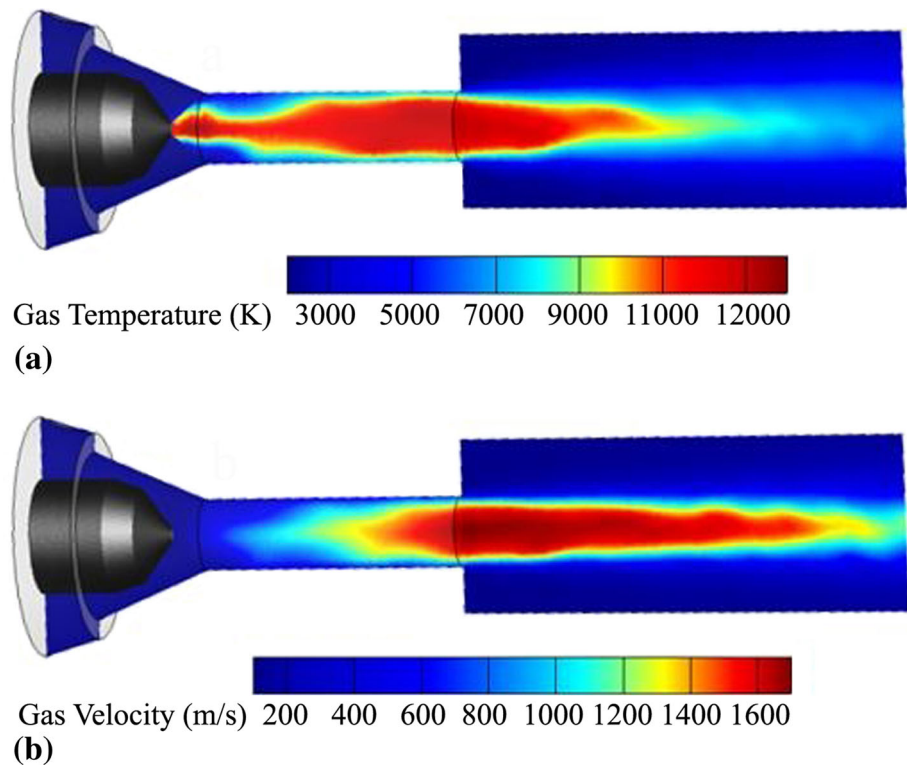

Gas Temperature (K)   3000   5000   7000   9000   11000   12000
(a)

Gas Velocity (m/s)   200   400   600   800   1000   1200   1400   1600
(b)

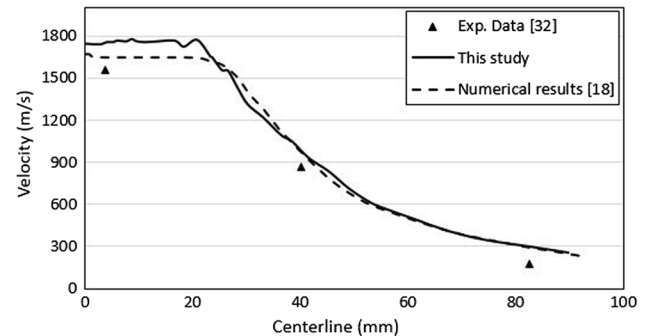**Fig. 12** Plasma gas temperature along the centerline

Fig. 13 Plasma gas velocity along the centerline

Unsteady Plasma Flow

In order to analyze the unsteady configuration results, the plasma gas temperature and velocity distributions at three different instants associated with three different voltages are shown in Fig. 14 and 15, respectively. To demonstrate the length of the plasma jet at these instants, an isosurface temperature of 11000 K and an isosurface velocity of 1600 m/s are selected, respectively.

Azimuthal fluctuations due to the plasma gas swirling having a counterclockwise rotation can be identified in Fig. 16 showing the plasma gas velocity contours at four different instants. The plane shown in Fig. 16 is selected at 6 mm from the gun exit which is the location of suspension injection.

The behavior of plasma jet due to both azimuthal and voltage fluctuations is represented in Fig. 17 at three different instants including the isosurface temperature of 11000 K. In Fig. 17, the streamlines are colored by plasma gas temperature and the arrows illustrate the rotation direction of the swirling gas flow, which is counterclockwise.

Discrete Phase

In the next step, results of the unsteady plasma jet are used to initialize the model with the suspension injection. Figure 18 illustrates the particle/droplet temperature distribution after the suspension injection and its interaction with the unsteady plasma jet. In this figure, an isosurface of gas

Fig. 14 Unsteady plasma gas temperature with a 600 A current and instantaneous arc voltage of (a) 62, (b) 50, and (c) 42 V
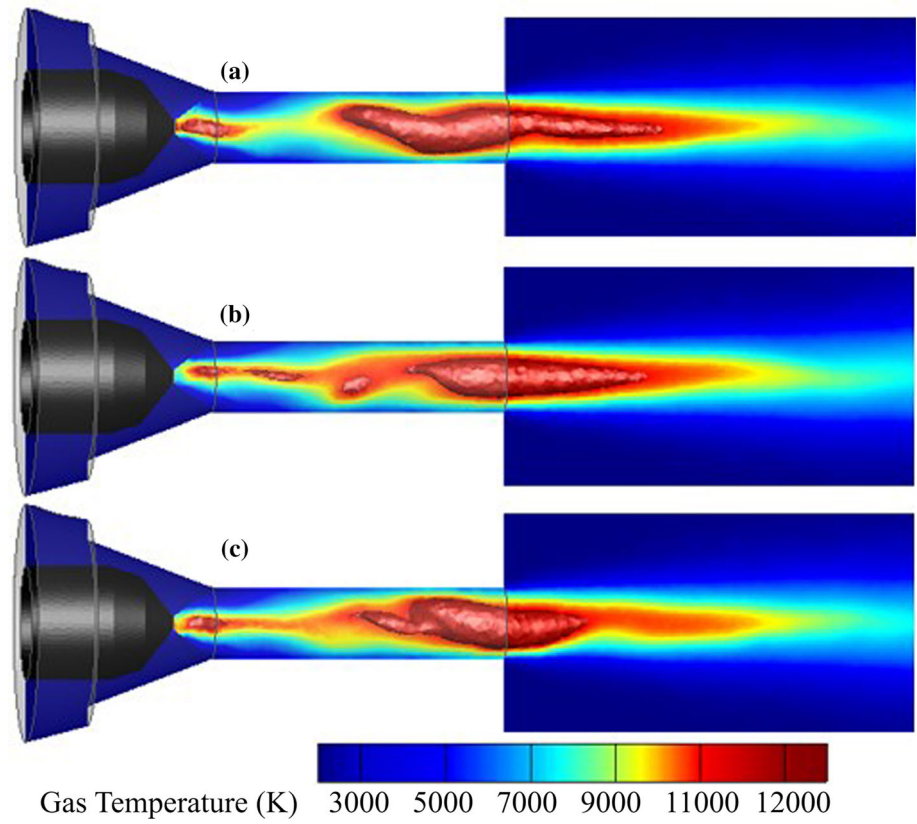
Gas Temperature (K)　3000　5000　7000　9000　11000　12000

Fig. 15 Unsteady plasma gas velocity with a 600 A current and arc instantaneous voltage of (a) 62, (b) 50, and (c) 42 V

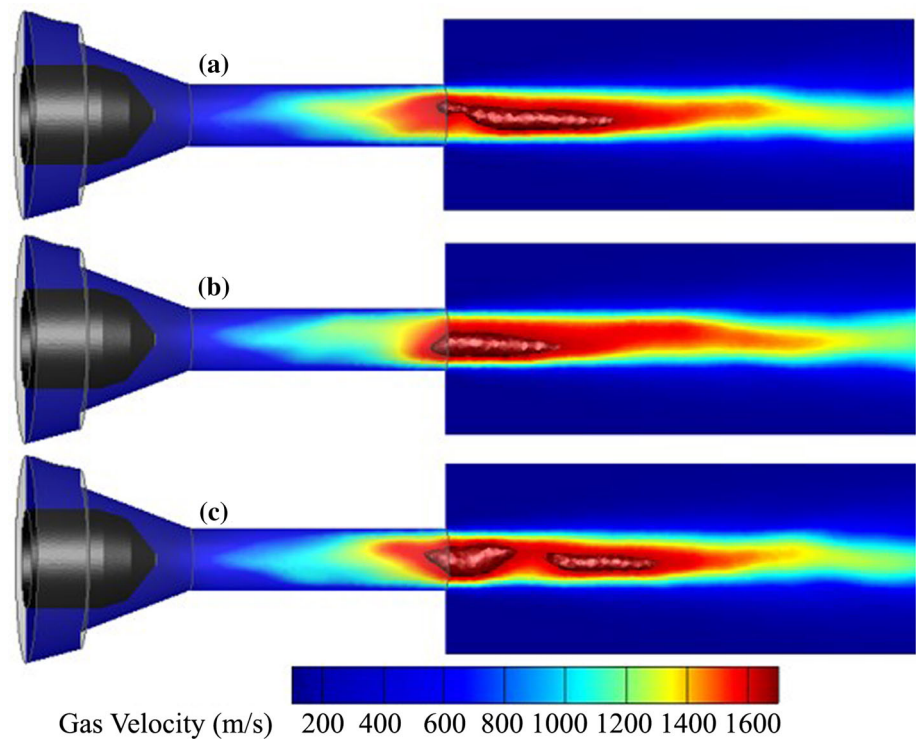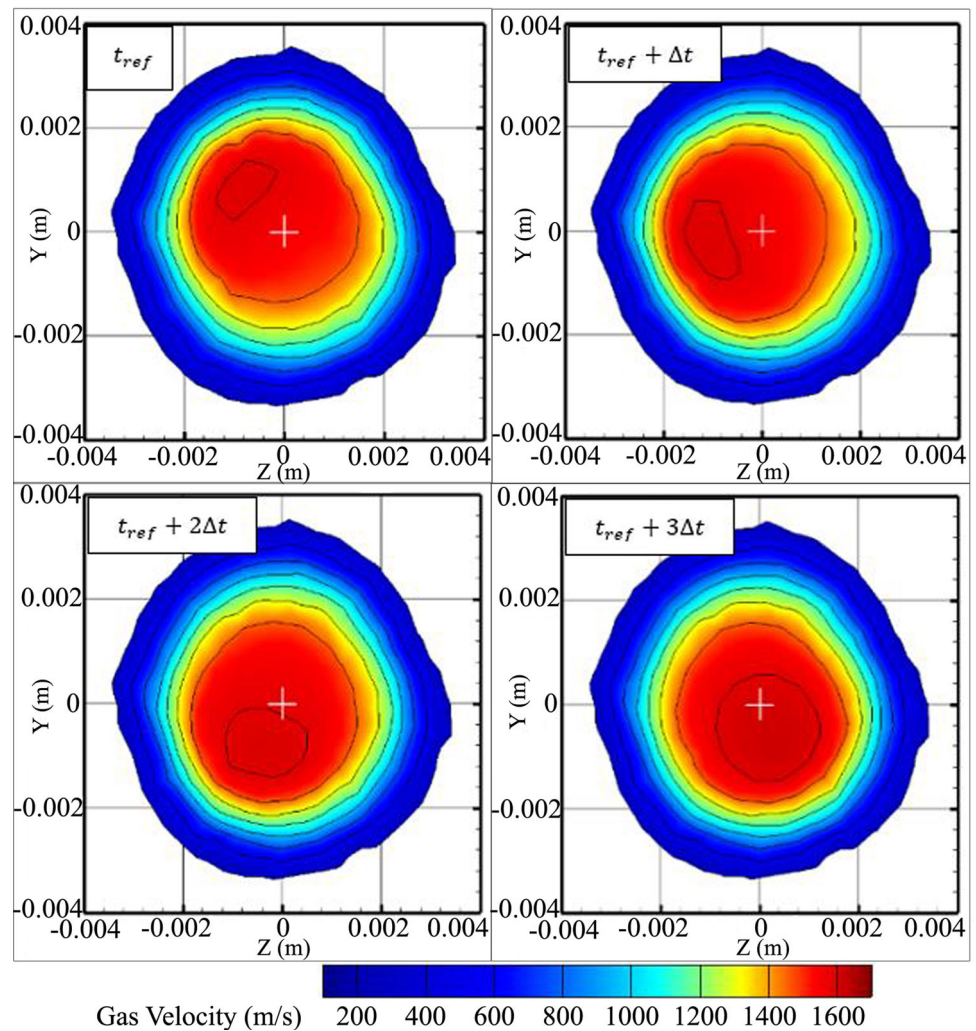Gas Velocity (m/s)　200　400　600　800　1000　1200　1400　1600

Fig. 16 Unsteady gas plasma velocity contours at a standoff distance of 6 mm from the gun exit at four snapshots

temperature equal to 10400 K is introduced to show the plasma jet oscillations at three different instants associated with voltages of 62, 56, and 46 V, respectively. The length of the outlet domain shown in Fig. 18 is taken to show the results with higher resolution due to investigating the distances of 40 and 60 mm from the gun exit.

Considering the flow parameters and the injector diameter (0.15 mm) as the initial size of the droplets, the calculated Weber number is between 300 and 520 at different locations in the plasma plume which justifies the use of the KH–RT breakup model in this study. It can be observed that fine particles located near the plasma torch centerline have gained higher temperature compared with the large blue droplets in which the ethanol is not fully evaporated due to their weak penetration in the plasma jet. These droplets are also shown in the figures. However, since the temperature of the particles is important to analyze the SPS process, the temperature bar illustrated in the

figures shows the temperature of the particles (i.e., solid or molten YSZ).

In order to better understand the effects of arc voltage fluctuations on particle properties, a more detailed analysis is carried out at two different distances (40 and 60 mm) from the gun exit. Figure 19 shows the plasma and particle temperatures at the three instants shown in Fig. 18 at 40 mm (a_1, a_2, and a_3) and 60 mm (b_1, b_2, and b_3) from the gun exit. Figure 20 represents the plasma and particles velocity at the same instants and locations.

Another important result, which can be concluded from Fig. 18, 19, and 20, is that at any given standoff distance, the particle temperatures and velocities vary in time due to the plasma oscillations. It can be seen that the majority of the particles are located in the left side of the cross sections shown in Fig. 19 and 20 due to the plasma jet counterclockwise rotation. Furthermore, it can be seen that the particle temperature, velocity, and position from the centerline are also changed significantly with time associated

Fig. 17 Streamlines colored by plasma gas temperature and isosurface temperature of 11000 K with current input of 600 A and arc voltages of (a) 62, (b) 51, and (c) 42 V (unsteady case)
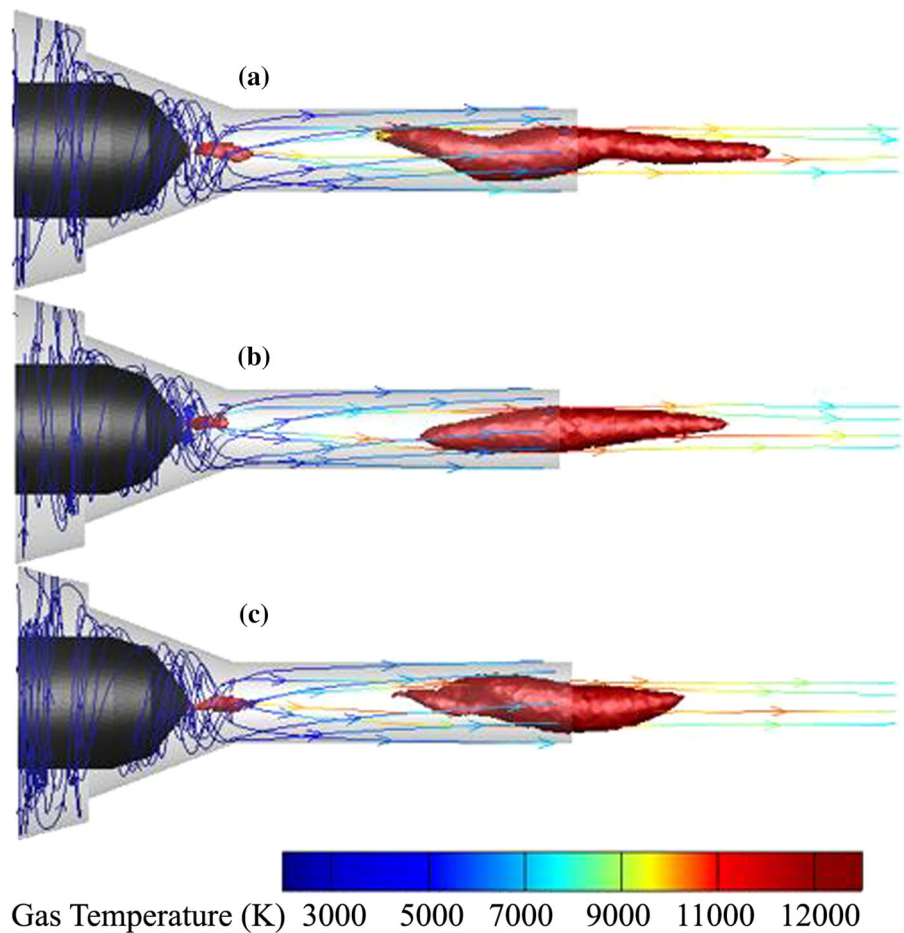
with the plasma jet fluctuations. Moreover, a wide range of particle size is observed again resulting from the plasma oscillations. Mostly at the plasma jet periphery, large, cold, and slow droplets are observed which correspond to suspension droplets in which the ethanol is not fully evaporated. Such droplets might cause imperfections in SPS coatings.

As a result of arc voltage fluctuations, particle temperature, velocity, and size distributions vary significantly with time. Therefore, in order to determine the actual distribution of these particle parameters, the time average of these distributions is calculated. Calculations are done inside a 25×25 mm^2 window centered on the gun axis at two different standoff distances.

The number of time steps taken into account (8 ms as the time step for a duration of 200 ms) is chosen in such a way that further increasing of time steps would not have a considerable effect on the particle characteristic distributions. The calculated distributions of particle temperature, velocity, and size at 40 and 60 mm from the gun exit are illustrated in Fig. 21 and 22, respectively. Figure 21 shows

that about 40% of the particles at a distance of 40 mm are in the molten state (melting point at 2988 K). By increasing the distance from the gun exit to 60 mm (Fig. 22), particle temperature drops and the percent of the molten particles decreases to 8%.

The results show a rather poor performance of the process due to the lack of suspension penetration and consequently far from an optimum heat and momentum exchange between plasma and suspension flows. This is consistent with the results obtained in (Ref 18).

Figures 21 and 22 also show the particles normal velocity distribution at both distances. It is obvious that the particle normal velocity decreases with increasing the distance from the gun exit. Decrease in the particle velocity could be explained by the decrease in the plasma gas velocity with the spray distance. As expected, the particles size distributions are quite similar at 40 and 60 mm as shown in Fig. 21 and 22. It can be expected for these results that locating the substrate at a distance closer to the torch exit (40 mm compared to 60 mm) can result in higher deposition efficiency and denser coatings as the particle

Fig. 18 Particle temperature and plasma gas temperature with a current input of 600 A and arc voltages of (a) 62, (b) 56 and (c) 46 V (unsteady case)
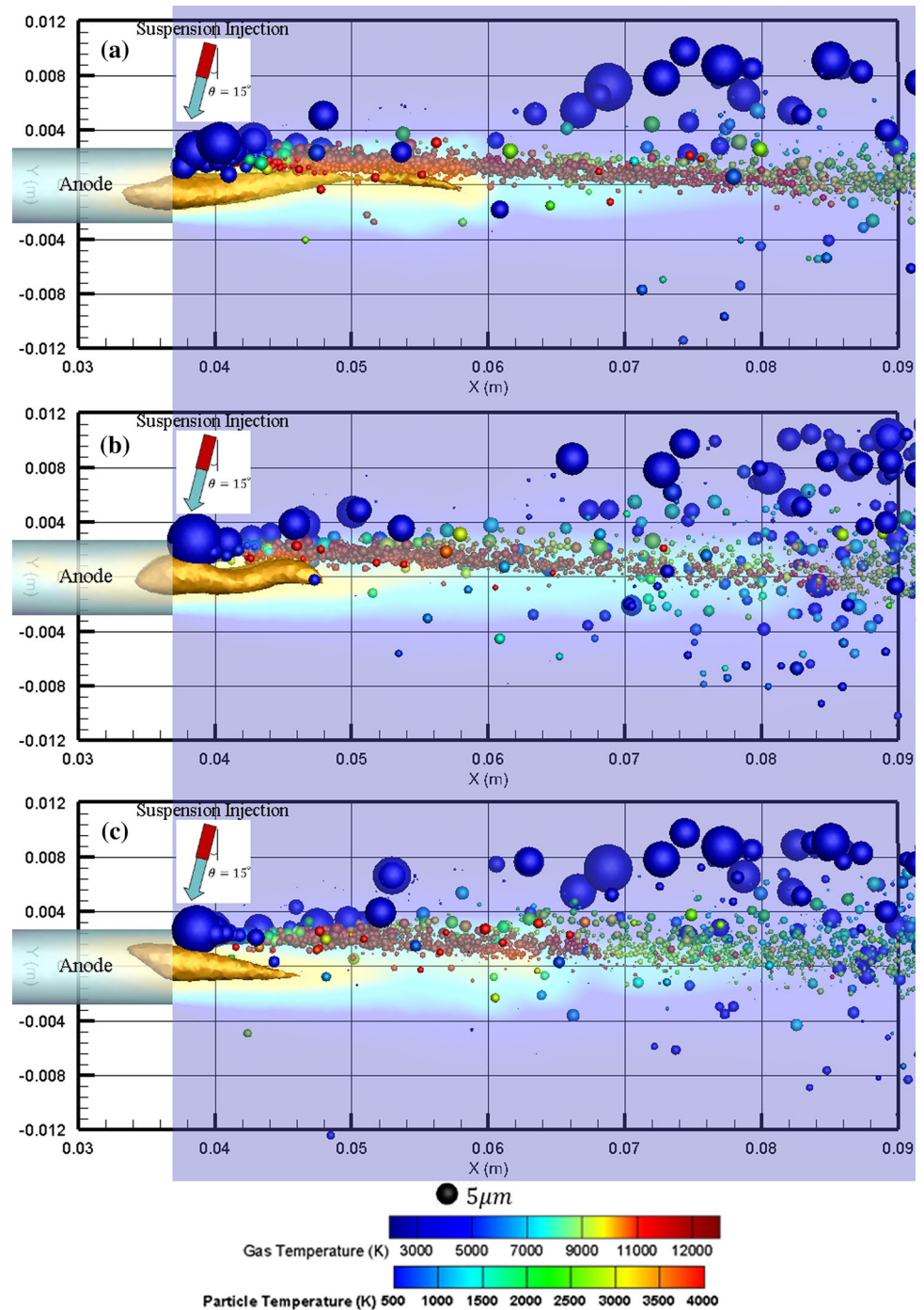
temperature and velocity are significantly higher at this shorter distance.

Effect of Changing the Suspension Feed Rate

The effect of changing the suspension mass flow rate on the particle trajectories and properties is also investigated. Figure 23 shows the interaction between the plasma jet and suspension injected at different mass flow rates of 22, 32, and 42 g/min. To show the plasma gas flow, a temperature isosurface equal to 10400 K is used.

In general, liquid jet penetration into a cross flow gas medium is dependent on the liquid-to-gas momentum flux ratio. By increasing the suspension flow rate (using the same injection diameter), the momentum flux ratio increases and consequently more jet penetration will occur.

Fig. 19 Particle temperature and plasma gas temperature at 40 mm from the gun exit with arc voltages of (a_1) 62, (a_2) 56, and (a_3) 46 V and at 60 mm from the gun exit with arc voltages of (b_1) 62, (b_2) 56, and (b_3) 46 V
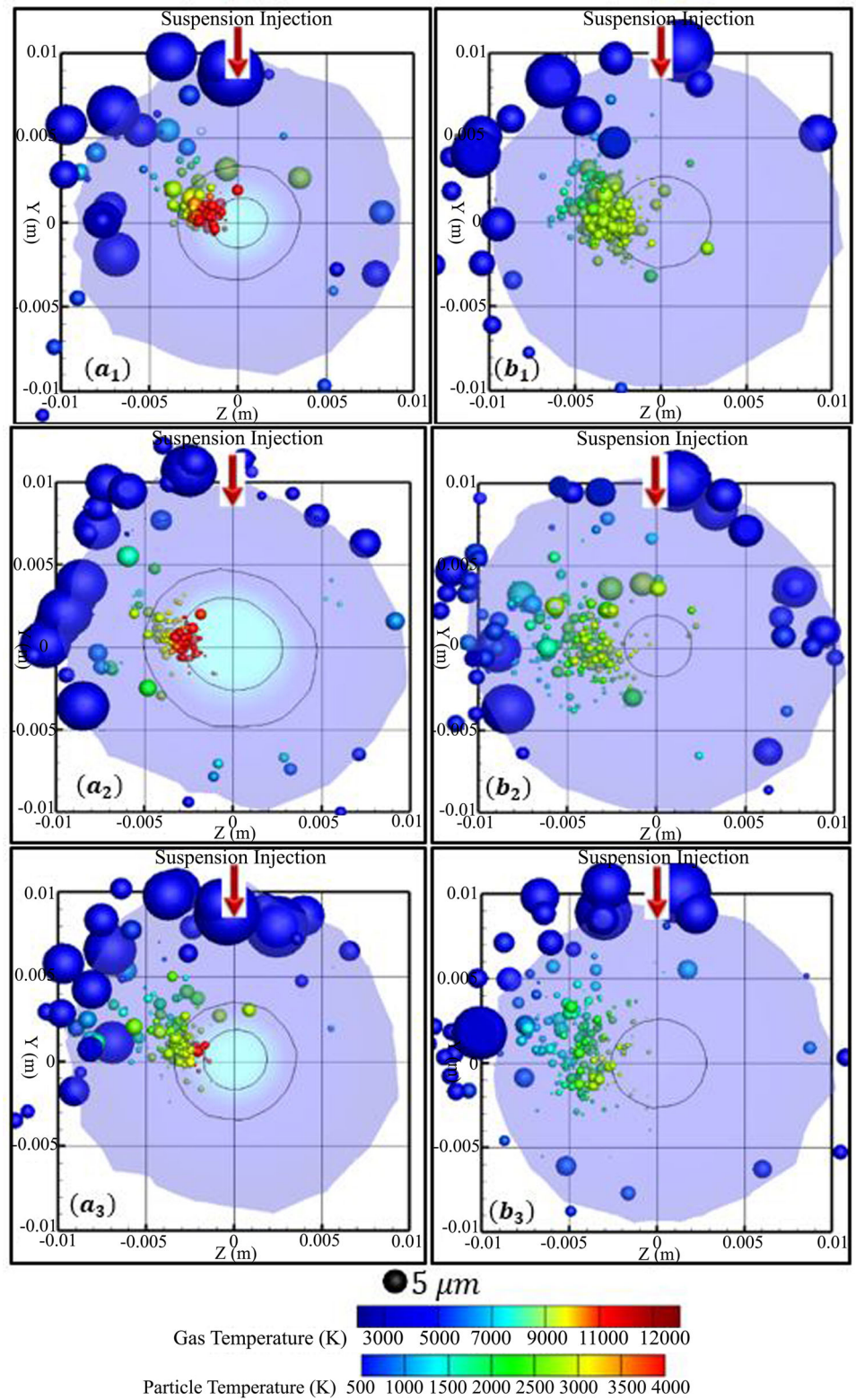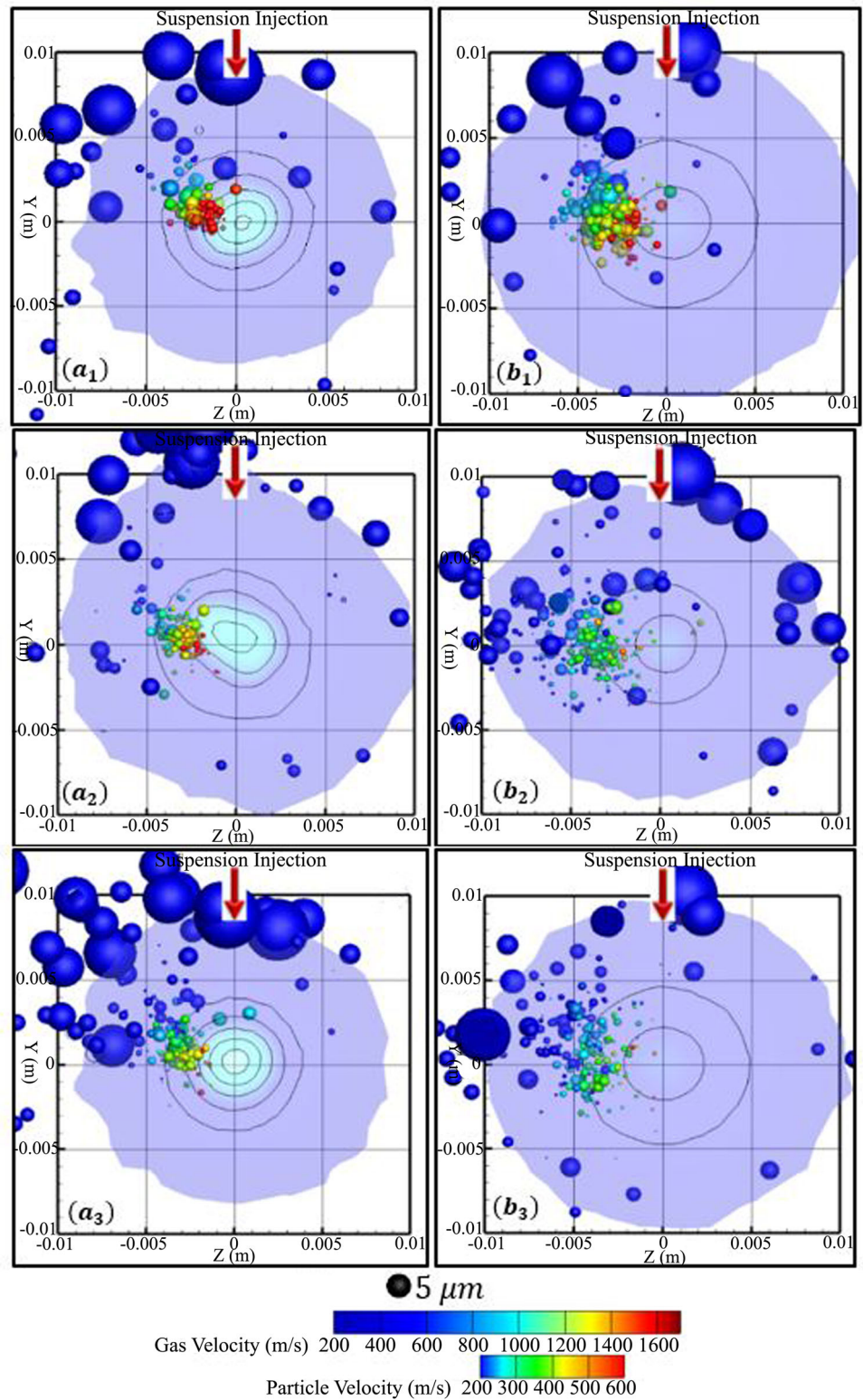
Fig. 20 Particle velocity and plasma gas velocity at 40 mm from the gun exit with arc voltages of (a_1) 62, (a_2) 56, and (a_3) 46 V and at 60 mm from the gun exit with arc voltages of (b_1) 62, (b_2) 56, and (b_3) 46 V

Fig. 21 Distribution of particle temperature, velocity, and size at a distance of 40 mm from the gun exit
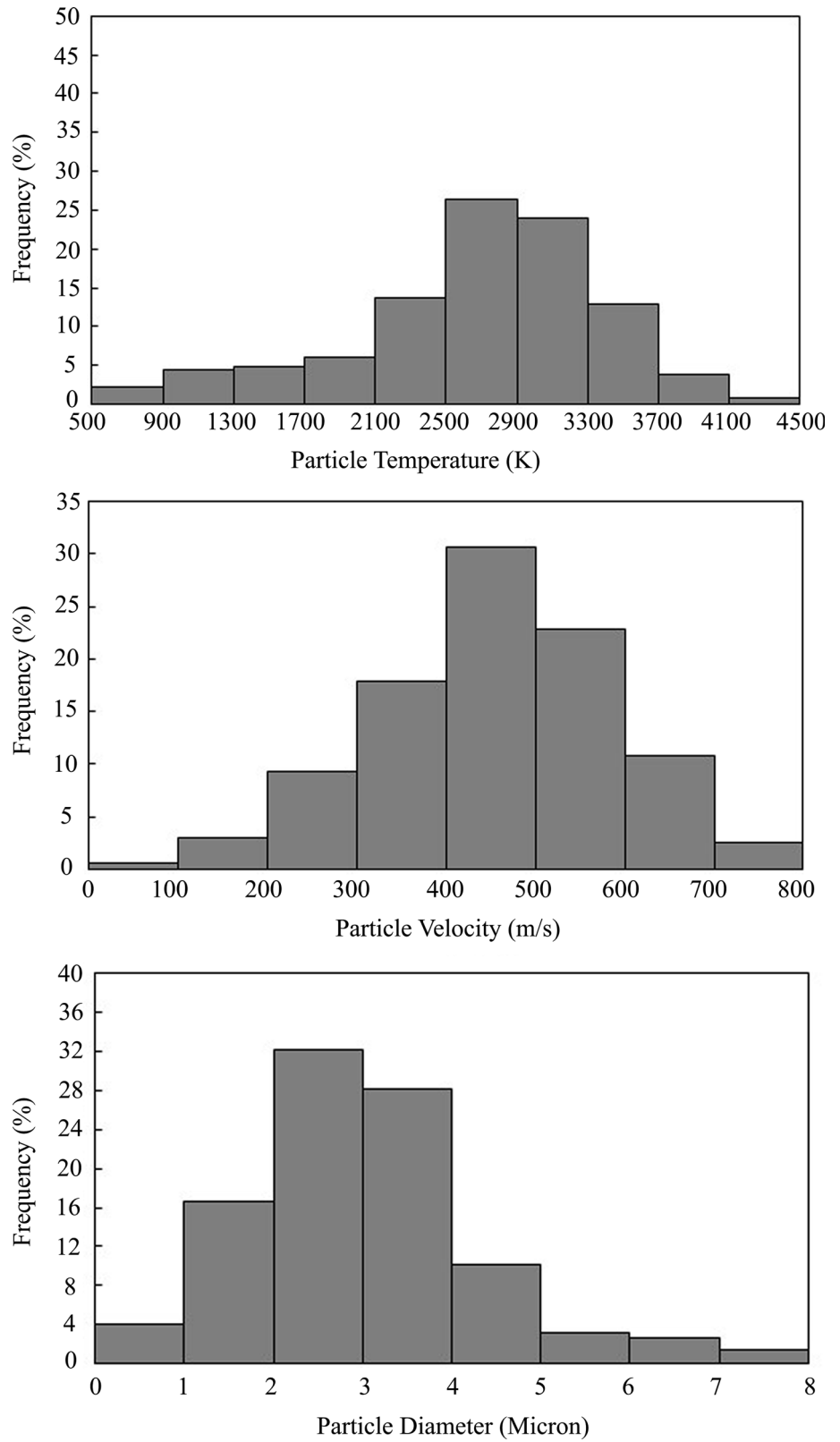
Fig. 22 Distribution of particle temperature, velocity, and size at a distance of 60 mm from the gun exit
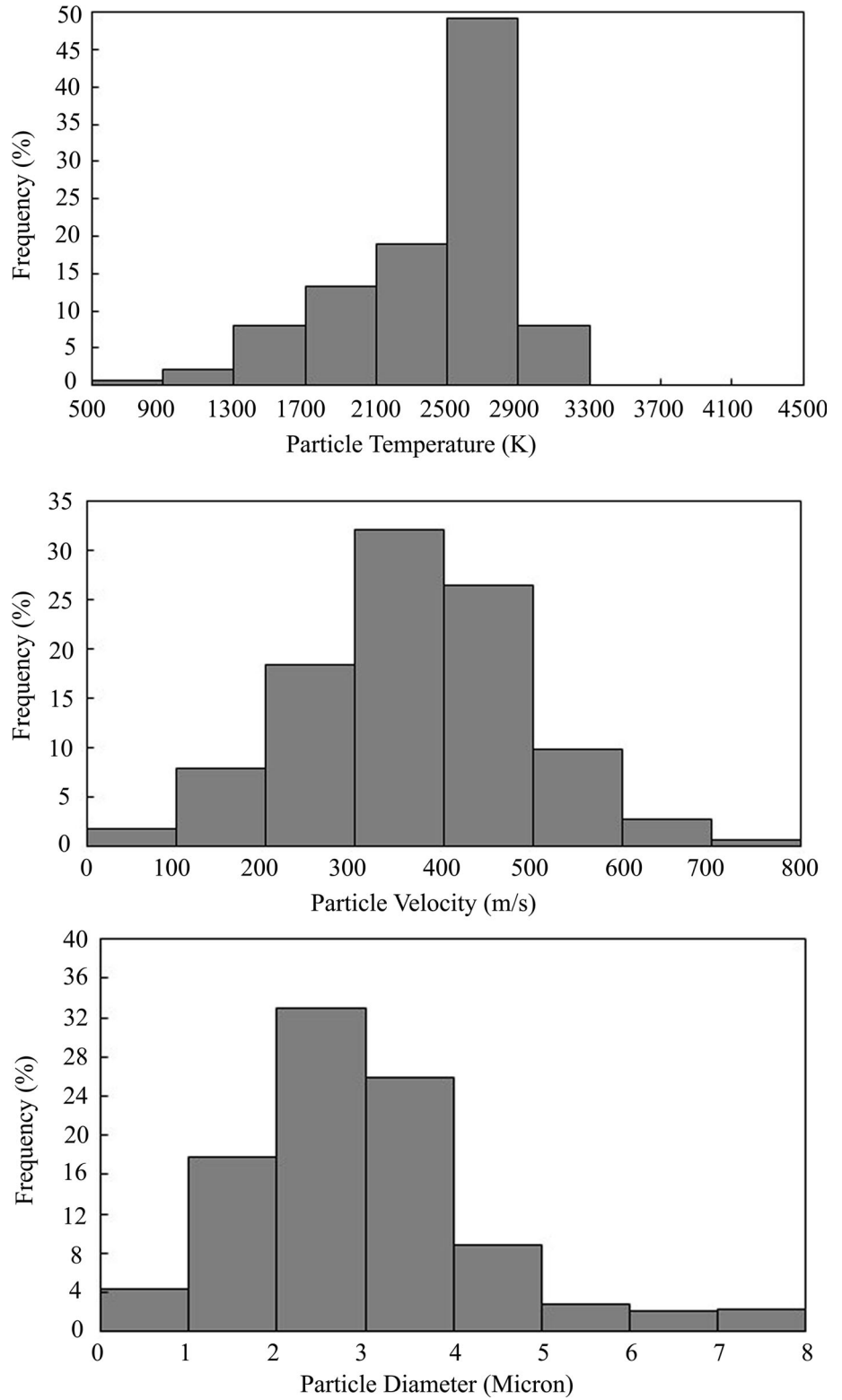
Fig. 23 Plasma gas and sprayed particle temperatures with suspension feed rates of (a) 22, (b) 32, and (c) 42 g/min
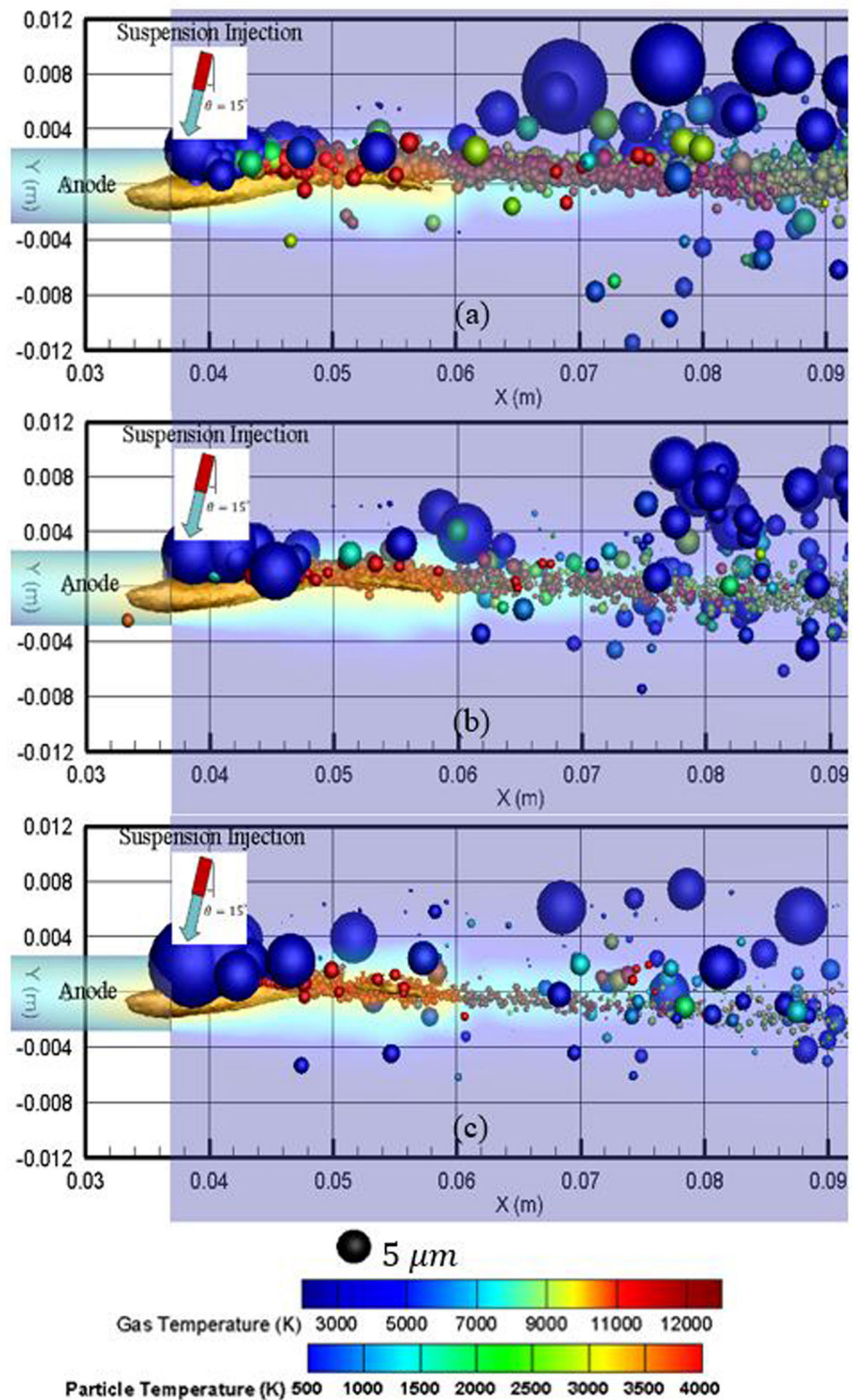
Fig. 24 Particle temperature distribution at a standoff distance of 40 mm with feed rates of (a) 22, (b) 32, and (c) 42 g/min
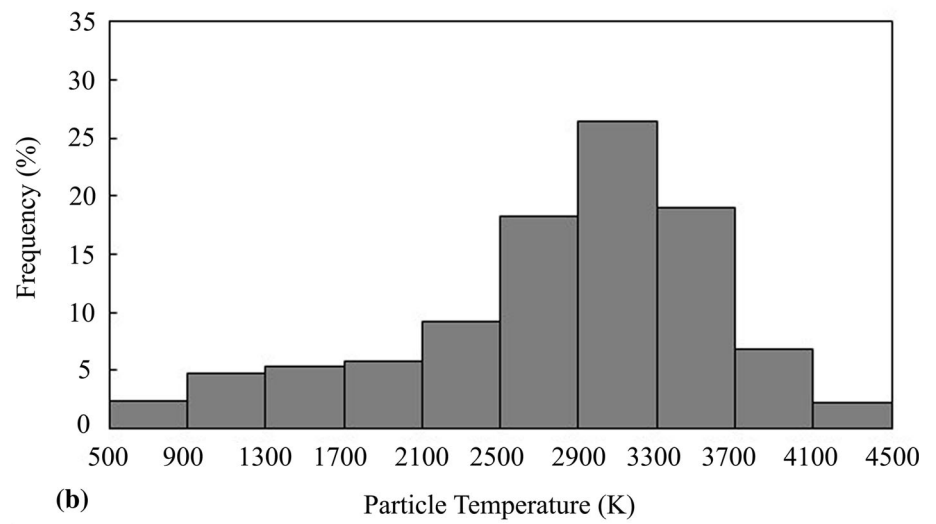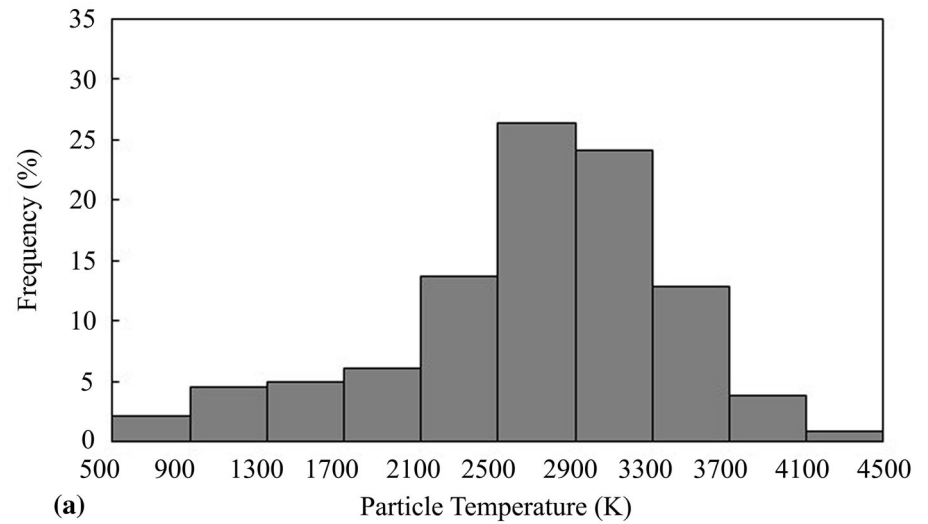

(a)

(b)

(c)
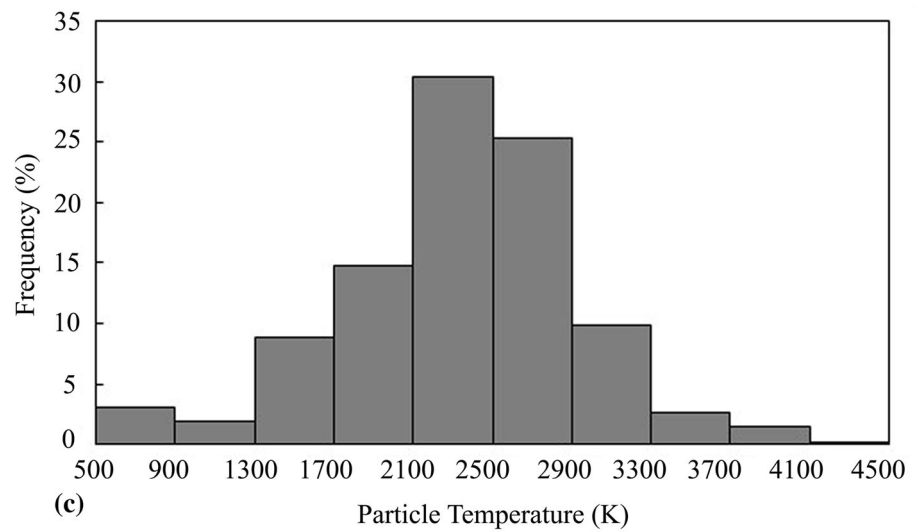
Fig. 25 Particles velocity distribution at a standoff distance of 40 mm with feed rates of (a) 22, (b) 32, and (c) 42 g/min
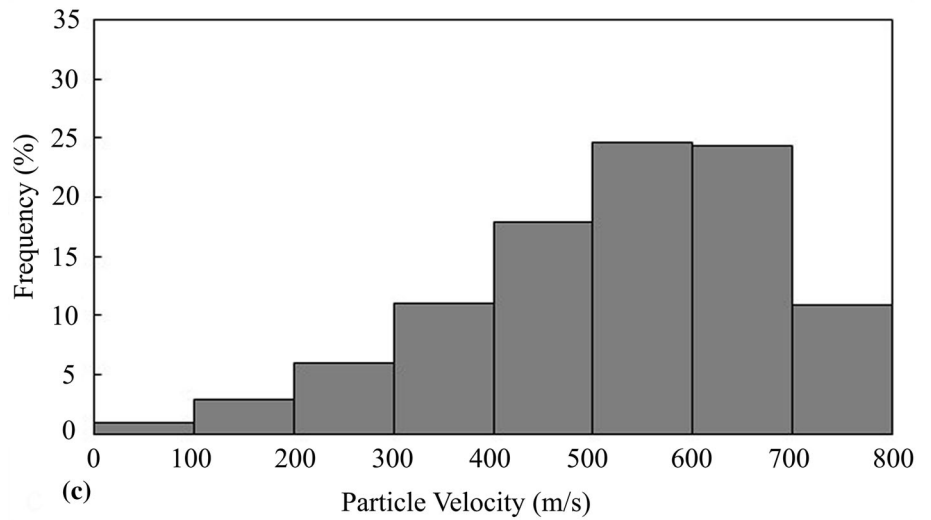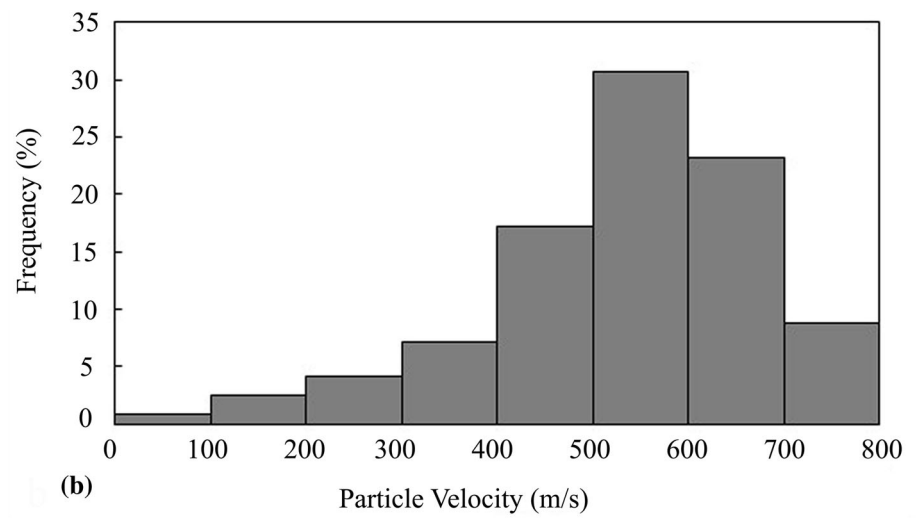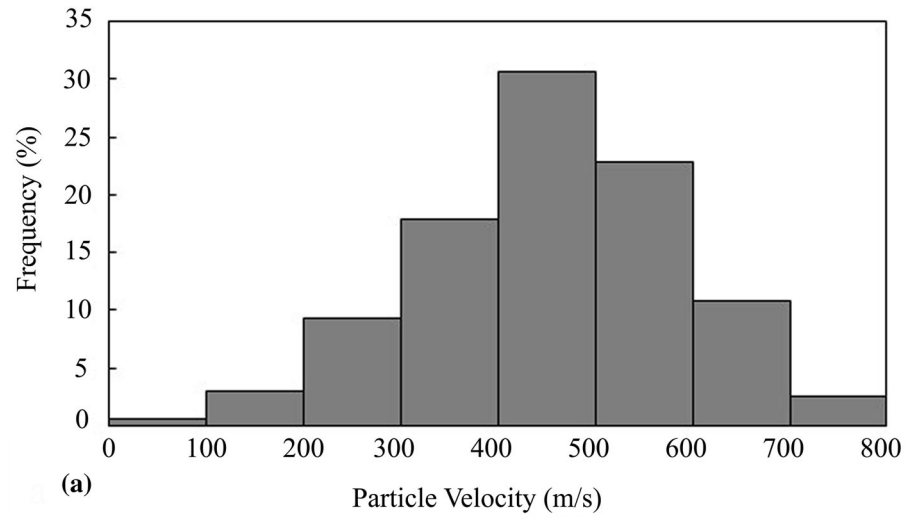
Fig. 26 Particles diameter distribution at a standoff distance of 40 mm with feed rates of (a) 22, (b) 32, and (c) 42 g/min
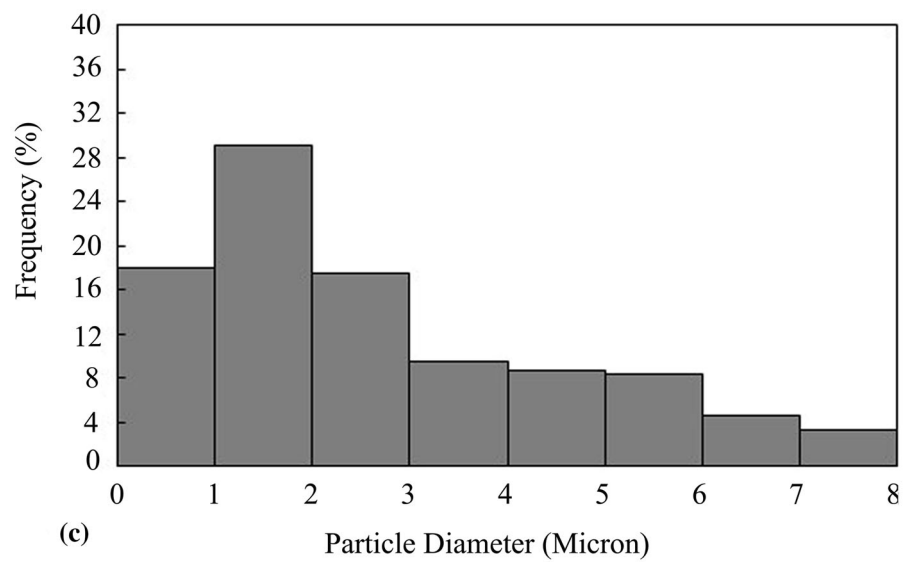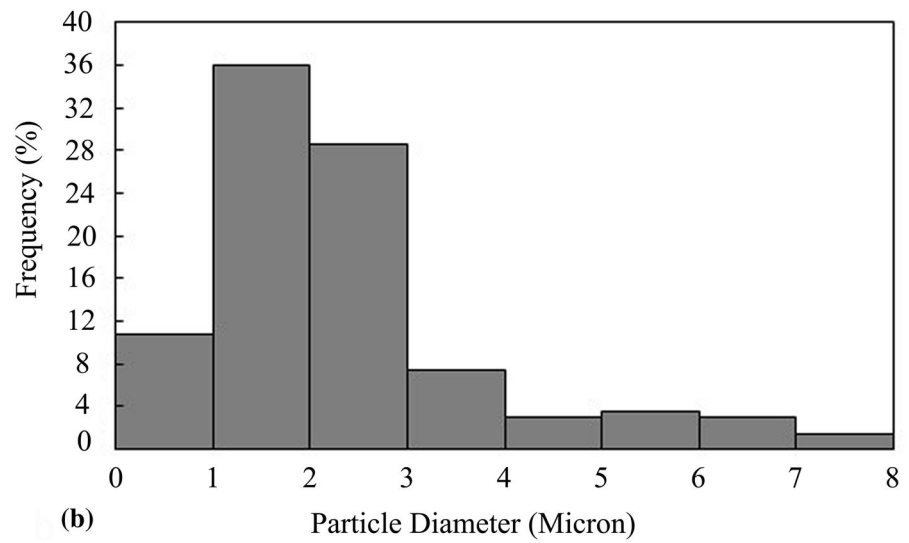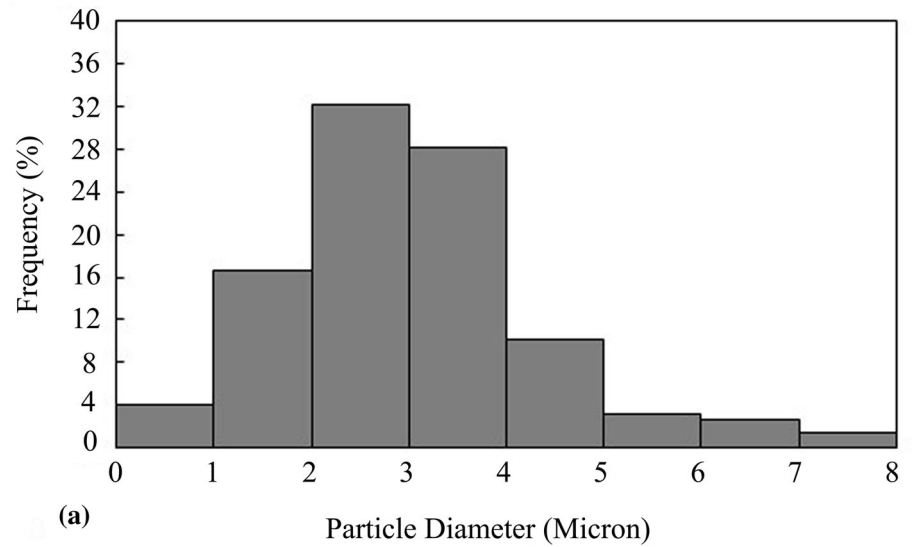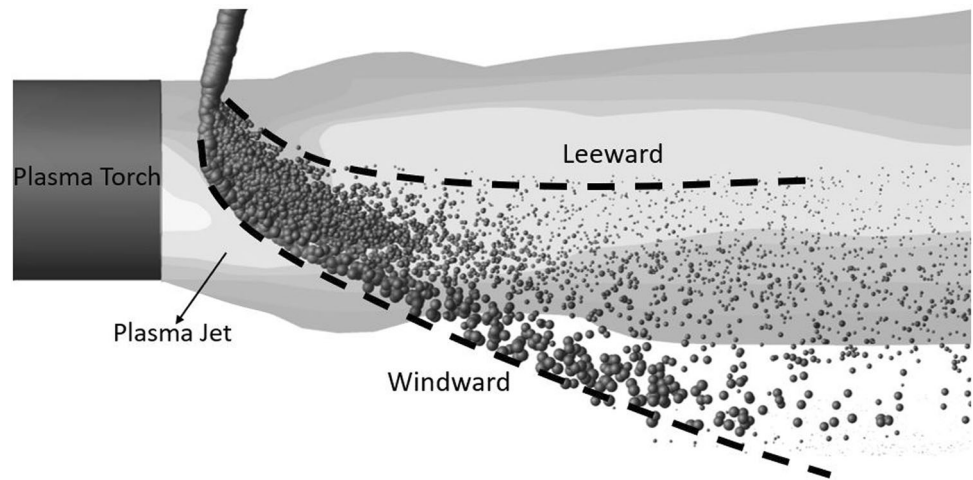
Fig. 27 Schematic of leeward
and windward trajectories

If the momentum flux ratio (in this case suspension feed rate) is too small, the suspension will not penetrate to the plasma core where the gas velocity is high, resulting in low droplet Weber number and consequently poor fragmentation or breakup. By adjusting the suspension feed rate to allow the majority of suspension droplets reach the centerline, one can expect finer atomization and also rapid evaporation of ethanol due to the high-temperature medium in the core of plasma plume. Further increase in suspension feed rate will result in an undesired configuration in which the suspension jet completely crosses the plasma plume.

It is observed that smaller particles are obtained in cases (b) and (c) compared with case (a). Having smaller particles is a consequence of a more efficient droplet fragmentation. Another important conclusion is that the number of cold particles is significantly decreased by increasing the suspension mass flow rate. This results from a better penetration of the suspension jet in the plasma jet at higher mass flow rate as the injection speed of the suspension is higher (same injector width). Moreover, the length of the high-temperature plasma gas decreases by increasing the suspension feed rate. In other words, the plasma jet is cooled down more in case (c) compared with cases (a) and (b) due to the increased momentum and energy exchange between the plasma plume and suspension flow.

Figures 24, 25, and 26 represent the sprayed particle temperature, velocity, and diameter distributions, respectively. The values in these figures are calculated from averaging the particles properties over time inside a 25×25 mm^2 window at the centerline at a standoff distance of 40 mm. It can be observed that in case (b), since the injected particles are closer to the centerline, they gain higher velocities compared with the two other cases.

Comparing different suspension mass flow rates in Fig. 24, 25, and 26 shows that the quantity of particles with higher temperature and higher velocity is maximum in case (b). In addition, increasing the suspension mass flow rate, as noted before, results in smaller particle size as shown in Fig. 26. The main reason is that larger instabilities on the droplet surface are developed due to the increased penetration of droplets to the plasma centerline, i.e., higher droplet Weber number.

As explained above, as a result of arc voltage fluctuations, the in-flight particle trajectory, temperature, velocity, and size vary with time. Penetration of particles can be analyzed using leeward and windward trajectories (Fig. 27). Windward and leeward trajectories generally refer to a location relative to the prevailing gas flow direction. Windward trajectory is located where it is exposed to the predominant gas flow. Contrarily, leeward trajectory is not exposed to the prevailing gas flow. In plasma spraying, windward trajectory represents the maximum penetration depth. In this study, to see the effect of fluctuations on the particles trajectory, windward trajectories obtained with different mass flow rates are used. Minimum and maximum trajectory lines calculated from the windward trajectory at different instants are shown in Fig. 28. It is shown that for high mass flow rates, the suspension may cross the plasma flow and cool it down dramatically. In other words, by increasing the suspension mass flow rate, the average penetration height increases.

Effect of Eliminating Voltage Fluctuations (Quasi-Steady Case)

In this section, the injection of suspension droplets in a quasi-steady plasma (no voltage fluctuation) is investigated. The comparison of minimum and maximum

Fig. 28 Windward trajectory of particles with mass flow rates of 22, 32, and 42 g/min
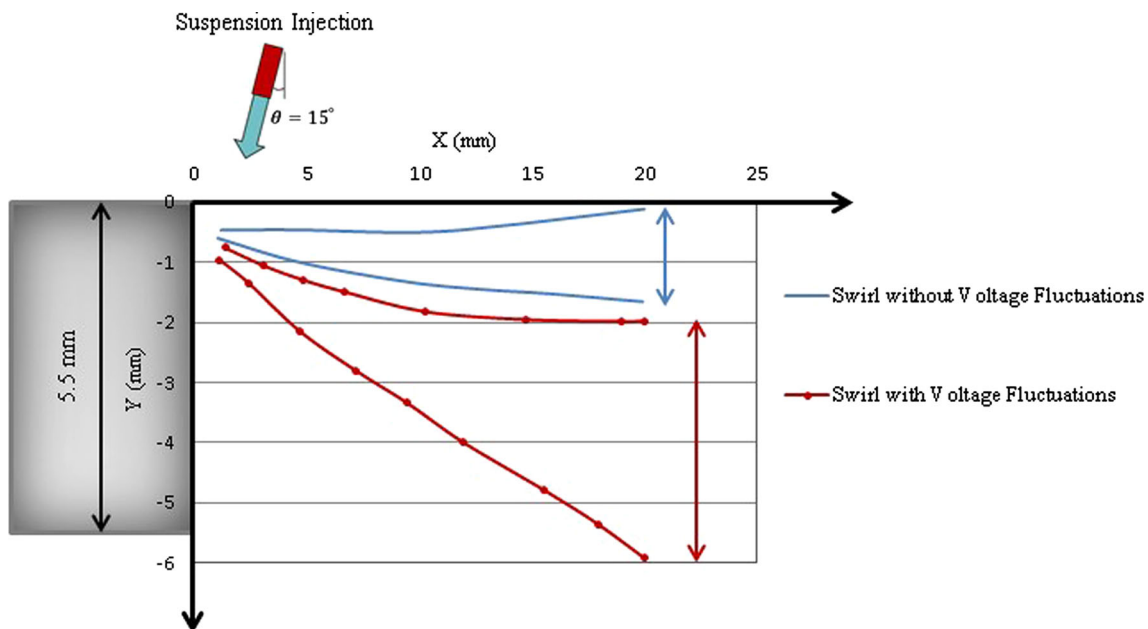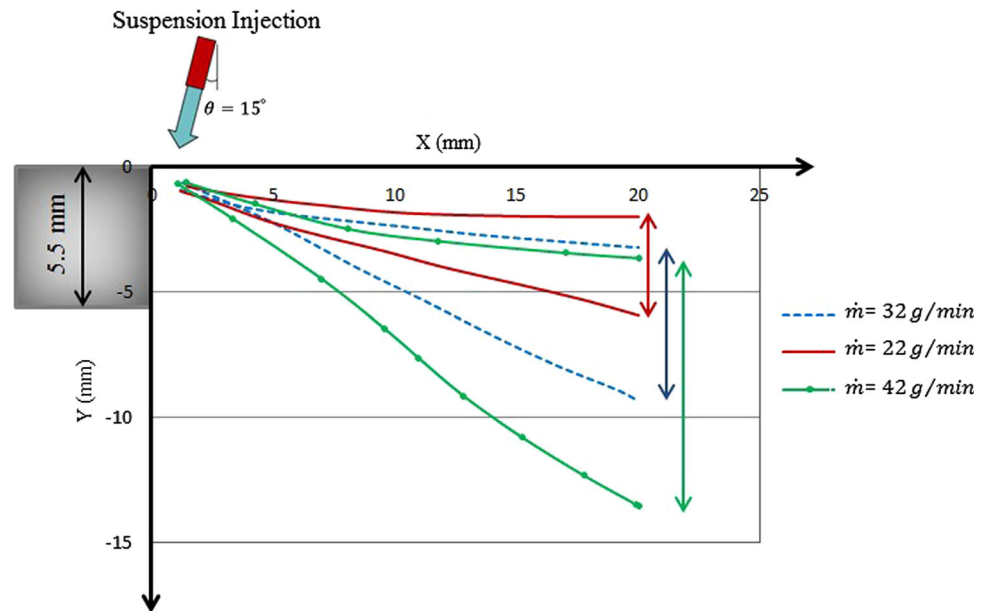

Fig. 29 Windward trajectory of particles in two cases of swirl without voltage fluctuations and swirl with voltage fluctuations (suspension mass flow rate is 22 g/min)

trajectories obtained from the windward trajectory with and without voltage fluctuations is shown in Fig. 29. It is evident that, in the presence of voltage fluctuations, the range of trajectories is much wider and the penetration is deeper in the plasma jet compared with the case with a constant voltage.

Particle temperature, velocity, and size distributions calculated inside a 25 × 25 mm² window across the gas flow at a distance of 40 mm from the gun exit with and

without voltage fluctuations are shown in Fig. 30, 31, and 32, respectively. In the case of constant voltage, the particles have lower temperature and velocity as compared to the case with arc voltage fluctuations due to the weaker suspension penetration. Indeed, in the quasi-steady case with constant voltage, the injected particles do not have the chance to penetrate into the centerline of the plasma plume contrary to the unsteady case with voltage fluctuations.

Fig. 30 Particles temperature distributions at a distance of 40 mm from the gun exit with swirl and (a) with voltage fluctuations, (b) without voltage fluctuations
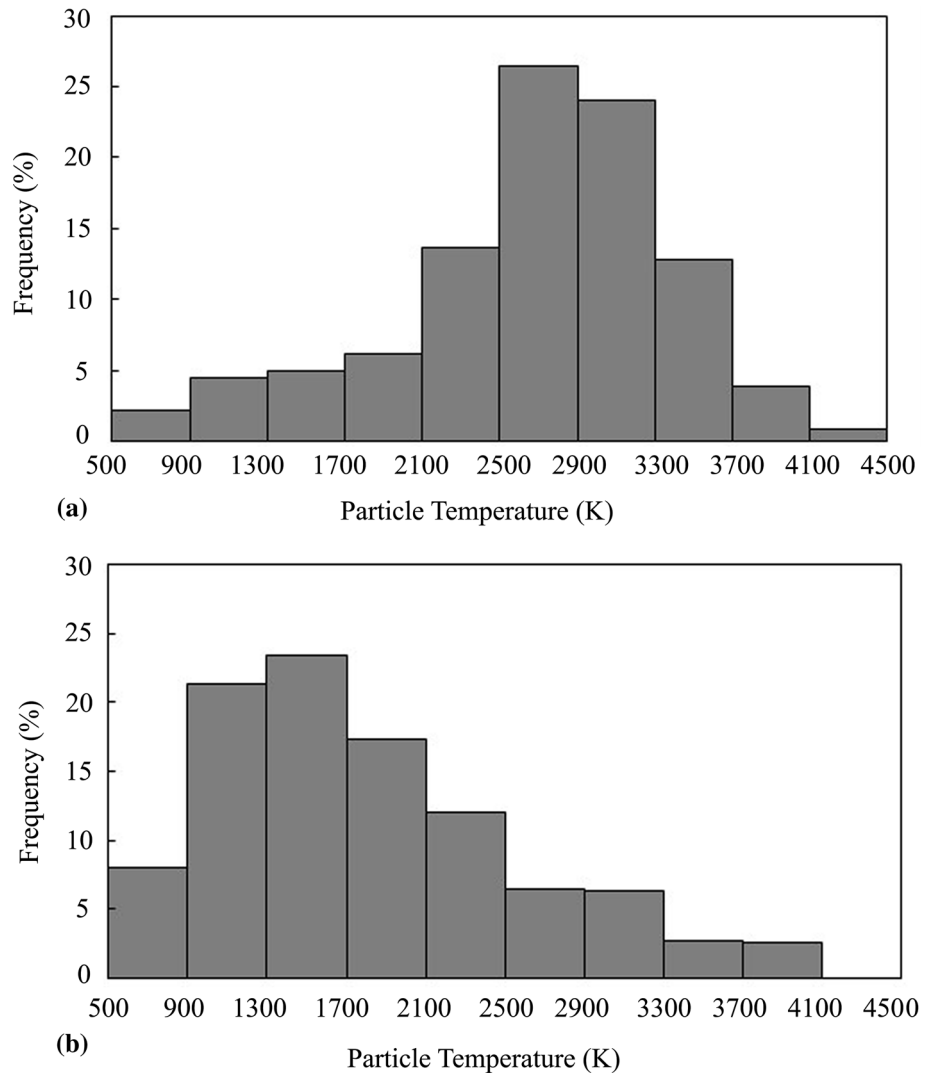
Conclusion

The aim of this research was to develop a more accurate plasma jet model for improving the simulation of the SPS process. The improved plasma jet model takes into consideration the azimuthal and axial fluctuations associated with the swirl and voltage fluctuations, respectively. This model was used to investigate the effect of oscillating plasma jet on the resulting particle properties. To do so, a three-dimensional numerical model of suspension plasma spraying has been developed and used to investigate the interaction between the plasma jet and the suspension flow. To model the oscillating plasma jet, a time-dependent heat source is introduced inside the plasma torch.

It was observed that the majority of the particles were diverted to the left side of the plasma jet as a result of the swirling plasma flow having a counterclockwise rotation. It was also shown that the fine particles closer to the plasma torch centerline have gained higher temperature compared with the other particles with larger size and lower temperature that experienced a much weaker penetration in the plasma jet.

The effect of changing the distance from the gun exit was investigated, and the results showed that locating a substrate in a distance closer to the torch exit (40 mm) compared with 60 mm results in higher particle temperature and velocity that can promote higher deposition efficiency and denser coatings.

Moreover, the effect of increasing suspension mass flow rate on the in-flight particles characteristics was investigated. It is observed that, by increasing the suspension feed rate, due to deeper penetration, droplets experienced more severe fragmentation resulting in smaller particle size. It is also shown that for high mass flow rates, the suspension may cross the plasma flow and cool it down dramatically. In other words, by increasing

Fig. 31 Particles velocity distributions at a distance of 40 mm from the gun exit with swirl and (a) with voltage fluctuations, (b) without voltage fluctuations
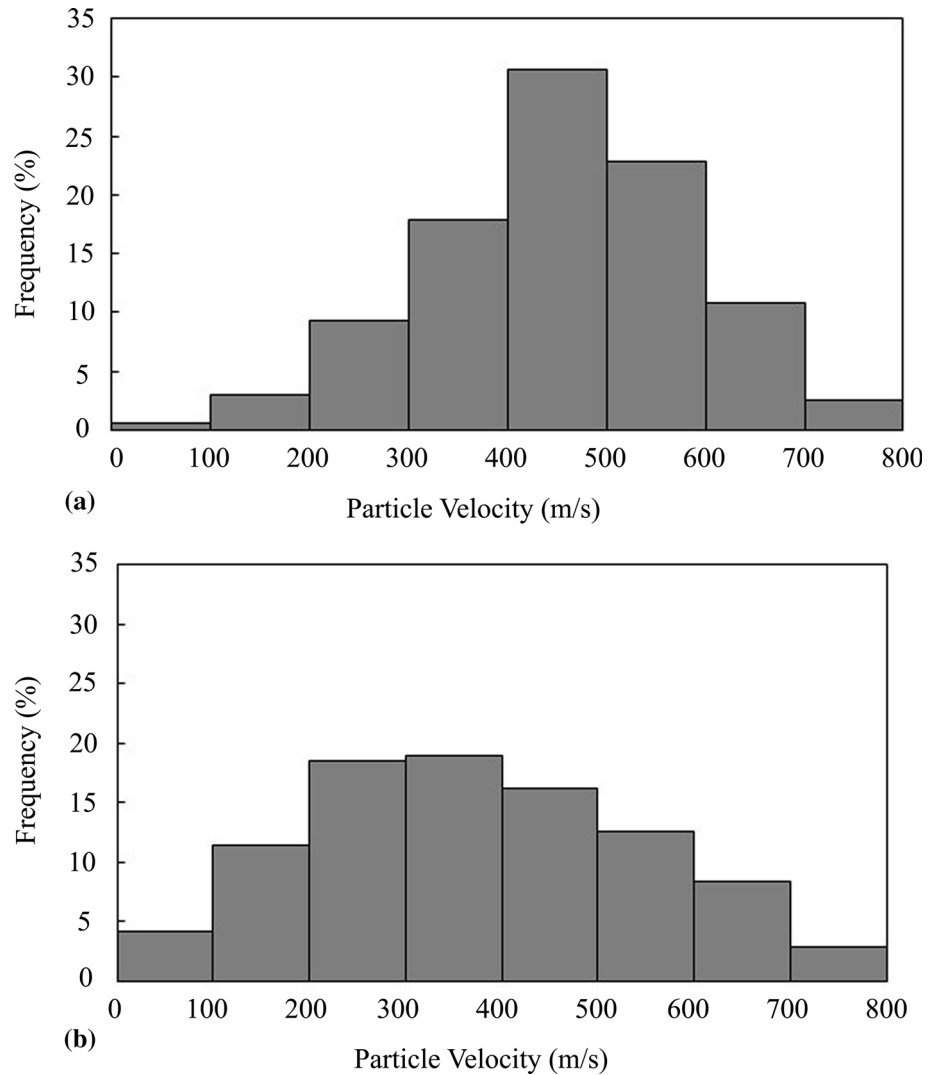

the suspension mass flow rate, the average penetration height increases.

Finally, the influence of the arc voltage fluctuations on the sprayed particle properties was investigated. The arc voltage fluctuations were found to cause more than two times wider particle trajectories resulting in wider particle temperature, velocity, and size distributions compared with the case of constant voltage.

It was also shown that, due to a better penetration of the suspension jet in the oscillating plasma jet (unsteady case), higher particle temperature and velocity as well as larger particle size are obtained compared with the quasi-steady case with a constant voltage. Based on these observations, it is obvious that the voltage fluctuations have a significant effect on the in-flight sprayed particles and, consequently, on coating quality.

Adding the experimental voltage fluctuations and the swirl in the model gave a more accurate representation of the plasma jet oscillations. However, since SPS is a very complex process, more work is necessary to better understand and model the influence of key physical and chemical phenomena involved from the plasma generation to the actual particle characteristics upon impact on the substrate. In particular, a more accurate method to simulate the oscillating plasma jet than the Joule effect method used in this study would be appropriate to obtain more precise results. Additionally, the influence of the injected particle diameter, angle of injector, anode erosion, etc. need to be further investigated as these factors affect the sprayed particle characteristics close to the substrate and then the resulting coating structure and properties.

Fig. 32 Particles diameter distributions at a distance of 40 mm from the gun exit with swirl and (a) with voltage fluctuations, (b) without voltage fluctuations

(a)

(b)
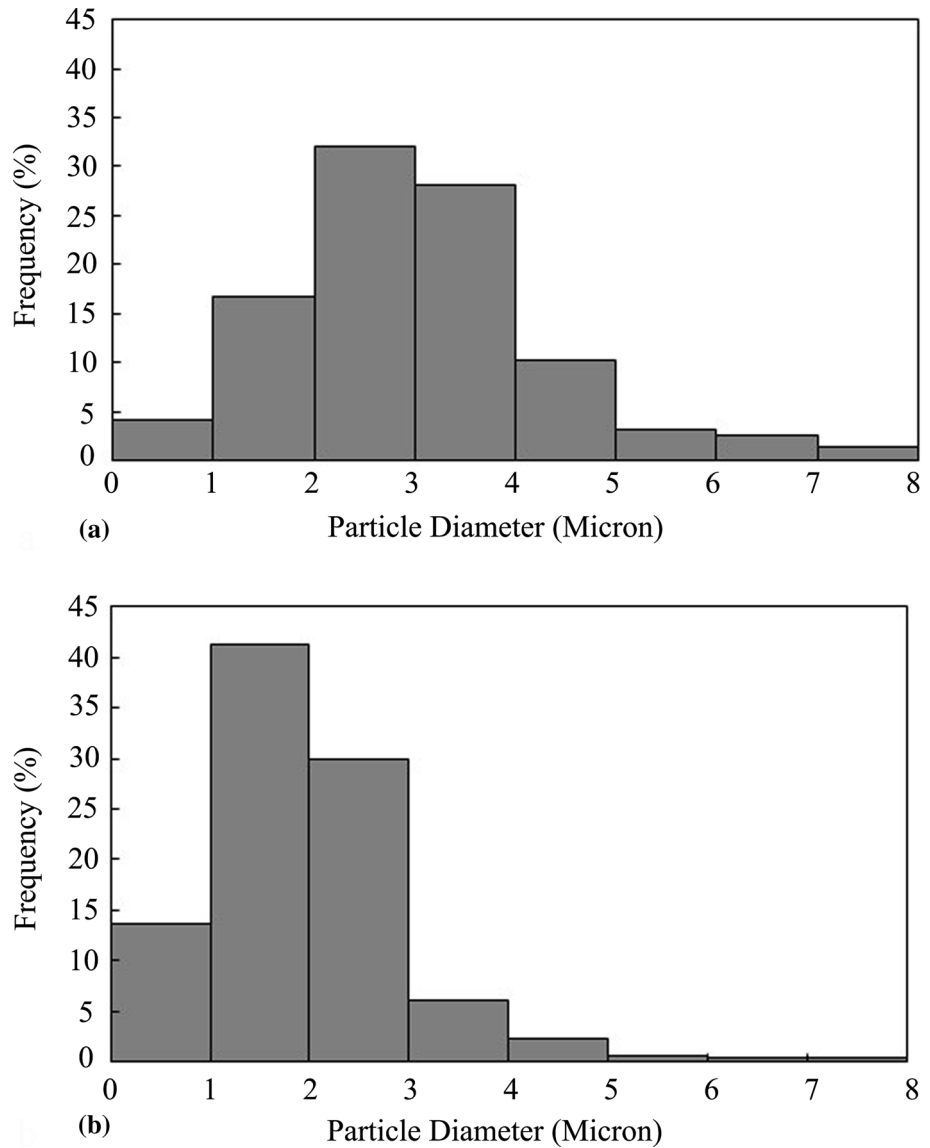
References

1. P. Fauchais, J. Heberlein, and M.I. Boulos, *Thermal Spray Fundamentals*, Springer, New York, 2014
2. A. Vardelle, C. Moreau, J. Akedo, H. Ashrafizadeh, C.C. Berndt, J. Oberste Berghaus, M. Boulos, J. Brogan, A.C. Bourtsalas, A. Dolatabadi, M. Dorfman, T.J. Eden, P. Fauchais, G. Fisher, F. Gaertner, M. Gindrat, R. Henne, M. Hyland, E. Irissou, B. Jodoin, E.H. Jordan, K.A. Khor, A. Killinger, Y.-C. Lau, C.-J. Li, L. Li, J. Longtin, N. Markocsan, P.J. Masset, J. Matejicek, G. Mauer, A. McDonald, J. Mostaghimi, S. Sampath, G. Schiller, K. Shinoda, M.F. Smith, A.A. Syed, N.J. Themelis, F.-L. Toma, J.P. Trelles, R. Vassen, and P. Vuoristo, The 2016 Thermal Spray Roadmap, *J. Therm. Spray Technol.*, 2016, **25**, p 1376-1440
3. A. Vardelle, C. Moreau, N.J. Themelis, and C. Chazelas, A Perspective on Plasma Spray Technology, *Plasma Chem. Plasma Process.*, 2015, **35**, p 491-509
4. J. Fazilleau, C. Delbos, V. Rat, J.F. Coudert, P. Fauchais, and B. Pateyron, Phenomena Involved in Suspension Plasma Spraying Part 1: Suspension Injection and Behavior, *Plasma Chem. Plasma Process.*, 2006, **26**(4), p 371-391
5. J. Berghaus, B. Marple, and C. Moreau, Suspension Plasma Spraying of Nanostructured WC-12Co Coatings, *J. Therm. Spray Technol.*, 2006, **15**(4), p 676-681
6. P. Fauchais, R. Etchart-Salas, C. Delbos, M. Tognonvi, V. Rat, J.F. Coudert, and T. Chartier, Suspension and Solution Plasma Spraying of Finely Structured Layers: Potential Application to SOFCs, *J. Phys. D Appl. Phys.*, 2007, **40**(8), p 2394-2406
7. H. Samadi, *A Thick Multilayer Thermal Barrier Coating: Design, Deposition, and Internal Stresses*, Ph.D. Thesis, Department of Materials Science and Engineering, University of Toronto, Canada, 2009
8. J.F. Bisson, B. Gauthier, and C. Moreau, Effect of Plasma Fluctuations on In-Flight Particle Parameters, *J. Therm. Spray Technol.*, 2003, **12**, p 38-43

9. J.F. Bisson and C. Moreau, Effect of Direct-Current Plasma Fluctuations on In-Flight Particle Parameters: Part II, *J. Therm. Spray Technol.*, 2003, **12**, p 258-264

10. F. Jabbari, M. Jadidi, R. Wuthrich, and A. Dolatabadi, A Numerical Study of Suspension Injection in Plasma-Spraying Process, *J. Therm. Spray Technol.*, 2014, **23**, p 3-13

11. M. Jadidi, M. Mousavi, S. Moghtadernejad, and A. Dolatabadi, A Three-Dimensional Analysis of the Suspension Plasma Spray Impinging on a Flat Substrate, *J. Therm. Spray Technol.*, 2015, **24**, p 11-23

12. Y.P. Wan, V. Gupta, Q. Deng, S. Sampath, V. Prasad, R. Williamson, and J.R. Fincke, Modeling and Visualization of Plasma Spraying of Functionally Graded Materials and Its Application to the Optimization of Spray Conditions, *J. Therm. Spray Technol.*, 2000, **10**, p 382-389

13. D. Khelfi, A. Abdellah El-hadj, and N. Ait-Messaoudène, Modeling of a 3D Plasma Thermal Spraying and the Effect of the Particle Injection Angle, *Revue des Energies Renouvelables CISM'08 Oum El Bouaghi*, 2008, p 205-216

14. A. Boussagol, G. Mariaux, E. Legros, A. Vardelle, and P. Nylen, 3-D Modeling of a D.C. Plasma Jet Using Different Commercial CFD Codes, in *Proceedings of 14th International Symposium On Plasma Chemistry, Orleans, France*, 2000

15. R.L. Williamson, J.R. Fincke, and C.H. Chang, A Computational Examination of the Sources of Statistical Variance in Particle Parameters During Thermal Plasma Spraying, *Plasma Chem. Plasma Process.*, 2000, **20**, p 299-324

16. K. Cheng, X. Chen, and W. Pan, Comparison of Laminar and Turbulent Thermal Plasma Jet Characteristics—A Modeling Study, *Plasma Chem. Plasma Process.*, 2006, **26**, p 211-235

17. J.R. Fincke, D.M. Crawford, S.C. Snyder, W.D. Swank, D.C. Haggard, and R.L. Williamson, Entrainment in High-Velocity, High-Temperature Plasma Jets. Part I: Experimental results, *Int. J. Heat Mass Transf.*, 2003, **46**, p 4201-4213

18. K. Pourang, C. Moreau, and A. Dolatabadi, Effect of Substrate and Its Shape on in-Flight Particle Characteristics in Suspension Plasma Spraying, *J. Therm. Spray Technol.*, 2016, **25**, p 44-54

19. P. Eichert, M. Imbert, and C. Coddet, Numerical Study of an ArH$_2$ Gas Mixture Flowing Inside and Outside a de Plasma Torch, *J. Therm. Spray Technol.*, 1998, **7**, p 505-512

20. R. Huang, H. Fukanuma, Y. Uesugi, and Y. Tanaka, Simulation of Arc Root Fluctuation in a DC Non-transferred Plasma Torch with Three Dimensional Modeling, *J. Therm. Spray Technol.*, 2012, **21**, p 636-643

21. E. Safaei Ardakani and J. Mostaghimi, Arc Fluctuation Modeling in Non Transferred Direct Current Argon Plasma Torch, in *22nd International Symposium on Plasma Chemistry*, Antwerp, Belgium, 2015

22. J.P. Trelles, E. Pfender, and J. Heberlein, Multiscale Finite Element Modeling of Arc Dynamics in a DC Plasma Torch, *Plasma Chem. Plasma Process.*, 2006, **26**(6), p 557-575

23. E. Moreau, C. Chazelas, G. Mariaux, and A. Vardelle, Modeling the Restrike Mode Operation of a DC Plasma Spray Torch, *J. Therm. Spray Technol.*, 2006, **15**, p 524-530

24. C. Chazelas, J.P. Trelles, I. Choquet, and A. Vardelle, Main Issues for a Fully Predictive Plasma Spray Torch Model and Numerical Considerations, *Plasma Chem. Plasma Process.*, 2017, **37**, p 627-651

25. E. Meillot, D. Guenadou, and C. Bourgeois, Three-Dimension and Transient D.C. Plasma Flow Modeling, *Plasma Chem. Plasma Process.*, 2008, **28**, p 69-84

26. E. Meillot, S. Vincent, C. Le Bot, F. Sarret, J.P. Caltagirone, and L. Bianchi, Numerical Simulation of Unsteady ArH2 Plasma Spray Impact on a Moving Substrate, *Surf. Coat. Technol.*, 2015, **268**(88), p 257-265

27. C. Marchand, A. Vardelle, G. Mariaux, and P. Lefort, Modelling of the Plasma Spray Process with Liquid Feedstock Injection, *Surf. Coat. Technol.*, 2008, **202**, p 4458-4464

28. M.I. Boulos, P. Fauchais, and E. Pfender, *Thermal Plasma: Fundamentals and Application*, Vol 1, Plenum Press, New York, 1994

29. C. Kang, H. Ng, and S. Yu, Comparative Study of Plasma Spray Flow Fields and Particle Behavior Near to Flat Inclined Substrates, *Plasma Chem. Plasma Process.*, 2006, **26**, p 149-175

30. ANSYS Inc., *ANSYS FLUENT Theory Guide*, USA, 2011

31. M. P. Planche, *Experimental Study of Fluctuating Plasma Jets*, Ph.D. Thesis, University of Limoges, France, 1995

32. O. Betoule, *Relationships Between the Distributions of Particle Velocity and Temperature and Coating Properties*, Ph.D. Thesis, University of Limoges, France, 1994